Plasma Sources Science and Technology

PAPER

Collision integrals of electronically excited atoms in air plasmas. I. N–N and O–O interactions

To cite this article: Wensheng Zhao *et al* 2023 *Plasma Sources Sci. Technol.* **32** 125002

IOP Publishing Plasma Sources Science and Technology
Plasma Sources Sci. Technol. **32** (2023) 125002 (28pp) https://doi.org/10.1088/1361-6595/ad0edf

Collision integrals of electronically excited atoms in air plasmas. I. N–N and O–O interactions

Wensheng Zhao[1,2], Qizhen Hong[1], Chao Yang[3], Quanhua Sun[1,2] and Yuan Hu[1,*]

[1] State Key Laboratory of High Temperature Gas Dynamics, Institute of Mechanics, Chinese Academy of Sciences, Beijing 100190, People's Republic of China
[2] School of Engineering Science, University of Chinese Academy of Sciences, Beijing 100049, People's Republic of China
[3] Wide Range Flight Engineering Science and Applications Centers, Institute of Mechanics, Chinese Academy of Sciences, Beijing 100190, People's Republic of China

E-mail: yhu@imech.ac.cn

Received 1 August 2023, revised 31 October 2023
Accepted for publication 22 November 2023
Published 6 December 2023

Abstract

The current work presents the collision integral data for N(^4S)–N(^4S, ^2D, ^2P) and O(^3P, ^1D, ^1S)–O(^3P, ^1D, ^1S) interactions in the temperature range of 500–50 000 K. The collision integrals are calculated based on high-quality potential energy curves (PECs) obtained from fitting the high-level *ab initio* calculation data in a wide energy range to the neural network (NN) functions. In the construction of PECs, the diabatic PECs are adopted when avoided crossings exist because the diabatic paths are much more likely to be followed for such situations. Moreover, the nonadiabatic transition effects are estimated to be negligible for PECs crossings. The accuracy of traditional analytical formulas to fit PECs are also examined. It is found that the collision integral calculations are sensitive to the accuracy of PECs and the NN based PECs overwhelm the others. The contribution of inelastic excitation exchange processes to the diffusion collision integrals are also computed by using an accurate evaluation of the differences of PECs for *gerade* and *ungerade* pairs of excited atoms. Finally, based on the new collision integral data, we calibrate the collision model parameters suitable for the widely used particle simulation methods. The collision integrals and collision models developed in this work can be used to support high-confidence simulations of weakly ionized air plasma problems.

Keywords: collision integrals, potential energy curves, air plasmas, N–N and O–O interactions, electronic excitation

1. Introduction

There are many emerging applications, such as hypersonic vehicles in Earth's atmosphere [1], air breathing electric propulsion [2], air plasma spray [3] and reactive high power impulse magnetron sputtering [4], in which the weakly ionized plasma involving the atomic nitrogen and oxygen species plays a crucial role. Taking the hypersonic flight for example [1], the peak gas temperature in front of a re-entry vehicle can reach about 10 000 to 50 000 K and thereby a layer of nonequilibrium plasma is formed, causing the well-known phenomenon of communication blackout. Due to the moderate high temperature, almost all the diatomic nitrogen and oxygen in air dissociate to the atomic nitrogen and oxygen (N and O) but the level of ionization is relatively weak. Therefore, the comprehensive understanding of transport properties of N and O, along with other thermochemical processes, is of paramount importance for accurately predicting such nonequilibrium weakly ionized plasma flows.

Transport properties are usually obtained by computing the collision integrals for the scattering of gas particles

* Author to whom any correspondence should be addressed.

according to the Chapman–Enskog theory [5, 6]. Considerable calculations of collision integrals for N and O have been carried out over the past few decades. Levin *et al* [7] calculated the collision integrals of N–N and O–O for temperature in the range of 250 to 100 000 K using a semi-classical method. Later the calculation of collision integrals for high temperature air species, including the N–N and O–O interactions, was made by Capitelli *et al* with a classical approach [8, 9]. Analytical formulae for fitting and interpolating the calculated collision integrals were also proposed. The classical approach demonstrated its high degree of accuracy in calculating collision integrals of high-temperature atomic species in comparison to the semi-classical or quantum methods. This has further been confirmed by the recent work of Buchowiecki and Szabo [10], which revealed that the collision integrals are insensitive to the cross-section structure. The collision integrals from the aforementioned works [7–9] have been widely used and provided great support for many applications such as reentry and laboratory plasmas [11]. However, it is noted that only the interactions involving ground state species, e.g. N(^{4}S) and O(^{3}P), were treated in these calculations.

For the temperature range of interest in this work, the role of excited state atoms can be very important. This can be seen by estimating the number of different excited state atoms at a specific temperature with the Boltzmann distribution ($N_j/N_i = (g_j/g_i)\, e^{-\Delta E_{ij}/kT}$), where N, g, k, T are the number of particle, degeneracy, Boltzmann constant and temperature, respectively, the subscripts i and j denote the ith and jth electronic level, and ΔE_{ij} is the energy of jth electronic level relative to that of the ith level. At 50 000 K, we have $N_1 \approx 1.44N_0$ and $N_2 \approx 0.65N_0$ for atomic nitrogen while $N_1 \approx 0.35N_0$ and $N_2 \approx 0.04N_0$ for atomic oxygen. In addition, it has been found that the electronically excited species can play an important role in many plasma applications, e.g. the post-shock flow properties [12], the speed of flame propagation in combustion [13], the discharge properties of capacitively coupled plasmas [14], etc. For more applications, one can refer to the recent monograph and the references therein [15].

Kustova and Puzyreva [16] evaluated the effects of electronic excitation on the specific heats and transport properties of N and N_2 with a generalized Chapman–Enskog method. The contribution of the electronic modes to the thermal conductivity of species is predicted to be critical in the temperature of 10 000–40 000 K. Moreover, the collision integrals are found to be very important for the correct prediction of the transport properties. The influence of collision diameters of excited states on the transport coefficients is later investigated by employing the approximate Slater formula [17, 18]. It is found that the role of varying diameters of excited states is significant for temperature greater than about 14 000 K. In addition, their calculations showed that the model of Hirschfelder [19] rather than the famous Eucken model for thermal conductivity should be used in high temperature gases with electrioncally excited species.

The calculations of collision integrals take the potential energy curves (PECs) as input. Consequently, the quality of PECs is a determining factor for the accuracy of collision integrals. The PECs are usually obtained by fitting the experimental data (the measured dissociation energies, spectroscopic turning points, collision cross sections, etc) and/or *ab initio* calculation results to analytical functions. For the N–N and O–O scatterings, the most commonly used functional forms include the exponential function, Lenard–Jones (LJ) and its improved form (ILJ), Stockmayer, Born–Mayer, Tang–Toennies, Hublurt–Hirschelder (HH), Murrell–Sorbie (MS), Morse and its modified form, as well as a combination of them [9, 20–25]. In the earlier works of collision integral calculations mentioned above, the experimental and *ab initio* calculated data available for function fitting were scarce and thus limited the accuracy of those PECs, especially for collisions participated by excited state atoms at high temperatures. In recent years, high-level *ab initio* quantum chemistry methods have become a reliable alternative to generate high accuracy potential energy data, especially for the temperature in much wider range than before. The high accuracy *ab initio* data are then used to parameterize high-quality PECs and assess the capabilities of conventional potential energy functions with relatively simple analytical forms.

Recently, Laporta *et al* [26, 27] calculated the *ab initio* PECs of the ground electronic state of N_2 and O_2, as well as the resonant electronic states of N_2^- and O_2^-. Their work yielded valuable insights into vibrational-excitation cross sections and rate coefficients for electron-nitrogen and electron-oxygen collisions. Buchowiecki and Szabo recently calculated the potential energy data for ground state hydrogen colliding with nitrogen in both ground and low lying excited states in a wide range of interacting distances and energies [28]. The collision integrals based on the high-quality PECs were obtained for temperature up to 30 000 K. The accurate description of PECs at small interatomic distances (equivalently large interacting energies) was found to be important for the accuracy of collision integral results at high temperatures. Moreover, it was concluded that the simple analytical functions were often insufficient to provide reliable collision integral calculations for high temperature situations. The high-level *ab initio* methods have also been applied to the O–O and N–N systems. Liu *et al* [29] carried out the high-level *ab initio* calculations for O(^3P, ^1D, ^1S)–O(^3P, ^1D, ^1S) and obtained potential energy data much closer to the available experimental data than previous calculations. However, their results were insufficient at the short-range repulsive region. Therefore, the impact of Rydberg configurations cannot be fully considered, resulting in inaccurate results for the high-lying electronic states [30–32]. Moreover, no collision integral for O–O has been calculated based on these new *ab initio* data. Most recently, Qin *et al* [33, 34] found that the widely used HH and modified Morse functions were incapable of fitting the *ab initio* data for the N(^4S)–N(^4S, ^2D, ^2P) interactions in a wide range of energy. Instead, the PECs based on the combined-hyperbolic-inverse-power-representation function were shown to have very high accuracy. The collision integrals up to 40 000 K were also calculated [34].

For collisions between atoms with different excitation state, the effects of resonant exchange on transport properties can be very important. Nyeland and Mason [35] adopted an asymptotic approach to calculating the excitation exchange diffusion collision integral. Taking the atomic nitrogen as an illustration, they made the first quantitative evaluation of the contribution of excitation exchange to the diffusion collision integral and thermal conductivity. The results showed that the thermal conductivity associated with diffusion was reduced by a factor of three due to the exchange interactions of excited N at 10 000 K. This asymptotic method was shown to be quite accurate and widely applied to study the effects of resonant excitation exchange on collision integrals of high-temperature air with the ever-improving PECs. Sourd *et al* [36] assessed the influence of $N(^2D)$ and $N(^2P)$ on the transport properties of nitrogen with the model potentials calibrated by experimental spectroscopic data. Laricchiuta *et al* [37–39] made comprehensive calculations on collision integrals of electronically excited atoms in air plasmas by employing suitable combination of exponential (and its modified form), Morse and HH functions guided by the experimental and *ab initio* information. These calculations showed that the contribution of the inelastic excitation exchange process to the diffusion collision integral usually exceeds the elastic contribution considerably at high temperatures.

The aim of this work is to present new collision integral data with very high accuracy for $N(^4S)$–$N(^4S, ^2D, ^2P)$ and $O(^3P, ^1D, ^1S)$–$O(^3P, ^1D, ^1S)$ interactions in a wide range of temperatures by: (1) using the high-quality PECs obtained from the high-level *ab initio* calculations and neural network (NN) fitting method; (2) including the contribution of excitation exchange interactions to the diffusion collision integrals. For the high-quality PECs, adequate short-range data have been calculated, and more Rydberg configurations are included in the *ab initio* calculations of O–O system. The NN method for PECs construction is known for its accuracy and efficiency of fitting large data sets as well as minimal requirement of human intervention during the training process. The superiority of NN PECs is demonstrated by comparing with the well known MS and HH models, which were considered to be the best general purpose atom-atom potentials [36, 40]. The inelastic resonant excitation exchange collisions are evaluated based directly on the high accuracy PECs, instead of the exponential functions used in previous works [35–37, 39–41]. The rest of this paper is structured as follows. Section 2 describes the methodology for collision integrals and the details of the PEC calculation. In section 3, the results of PECs and collision integrals are presented and discussed. Finally, we conclude this study with section 4. Finally, the conclusions are in section 4.

2. Methodology

2.1. The calculation of collision integrals

The classical mechanical approach is used to calculate the cross sections, since it has comparable accuracy with the semiclassical WKB (Wentzel–Kramers–Brillouin) method, as indicated by [10]. Moreover, given that the collision integrals are insensitive to the cross-section structure and the resonance scattering mainly occurs at low energies, we exclude resonance scattering from our analysis in this work. For the elastic collision between atoms, the scattering angle can be related to the potential energy function $V(r)$ as follows [42]

$$\chi(\gamma, b) = \pi - 2b\int_{r_m}^{+\infty} \frac{\mathrm{d}r/r^2}{\sqrt{1-(b/r)^2 - V(r)/kT\gamma^2}}, \quad (1)$$

where b is the impact parameter, r_m is the distance of closest approach during the collision, R is the internuclear distance, and $\gamma = \sqrt{m_r g^2/2kT}$ (m_r-reduced mass, g-relative velocity, k-Boltzmann constant, T-temperature). Collision integrals are then expressed as [6, 28]

$$\sigma^2\Omega^{(l,s)*} = \frac{4}{(s+1)!\left[1-\frac{1}{2}\left(\frac{1+(-1)^l}{1+l}\right)\right]} \times \int_0^\infty \int_0^\infty \mathrm{e}^{-\gamma^2}\gamma^{2s+3}\left(1-\cos^l\chi\right) b\mathrm{d}b\mathrm{d}\gamma. \quad (2)$$

In this work, equation (2) are numerically integrated by using the code of O'Hara and Smith [43]. The code can efficiently handle the singularities in equation (2) by change of variables. In addition, the numerical integration is carried out in dimensionless coordinates to reduce the numerical error [44].

Furthermore, the inelastic resonant excitation-exchange processes are needed to be considered in the calculation for diffusion-type (or more exactly, the odd-order) collision integrals, i.e. the collisions between $N(^4S)$–$N(^2D,^2P)$, $O(^3P)$–$O(^1D,^1S)$, and $O(^1D)$–$O(^1S)$. For $N(^2D)$–$N(^2P)$ interaction, the inelastic contribution to the whole collision integrals is small [36] and thus not considered in this work. According to a semiclassical approach, the equation of inelastic diffusion-type collision integral $\sigma^2\Omega_{ex}^{(1,1)*}$ can be expressed as [35, 45]

$$\sigma^2\Omega_{ex}^{(1,1)*} = 4\pi\int_0^\infty \int_{b'}^\infty \mathrm{e}^{-\gamma^2}\gamma^{2s+3}\left(b'^2/4 + \sin^2(\theta)\, b\right)\mathrm{d}b\mathrm{d}\gamma, \quad (3)$$

where b' is the largest value of b for which $\theta(b)$ equals $\pi/2$, and

$$\theta = \frac{1}{\hbar g}\int_b^\infty \frac{|V_g(r) - V_u(r)|}{(r^2-b^2)^{\frac{1}{2}}} r\mathrm{d}r, \quad (4)$$

where $\hbar$ is reduced Planck constant, and the $V_g(r)$ and $V_u(r)$ are the potential energy functions for a pair of symmetric *gerade* and antisymmetric *ungerade* terms of molecular states. Equation (3) is integrated numerically. In particular, the variables r, b and g are change to $-2\sqrt{1-(b/r)^2}+1$, $2b'/b-1$ and $2/(g+1)-1$ in order to handle the singularity in the integration.

The final elastic or inelastic collision integrals can be obtained by averaging the contributions coming from the different PECs (with statistical weights p_n, which are equal to the

spin multiplicity for Σ molecular states and two times the spin multiplicity for the non-Σ molecular states) arising from the atom-atom interaction [46], i.e.

$$\langle \sigma^2 \Omega^{(l,s)*} \rangle = \frac{\Sigma_n p_n \sigma^2 \Omega_n^{(l,s)*}}{\Sigma_n p_n}, \tag{5}$$

where n denotes different molecular electronic states. The overall diffusion collision integrals $\sigma^2\Omega^{(1,1)*}$ that include both elastic and inelastic contributions are evaluated as follows [37],

$$\langle \sigma^2 \Omega^{(1,1)*} \rangle = \sqrt{\langle \sigma^2 \Omega_{el}^{(1,1)*} \rangle^2 + \langle \sigma^2 \Omega_{ex}^{(1,1)*} \rangle^2}. \tag{6}$$

In order to precisely describe the PECs appeared in equations (1) and (4), the NN method [47] is used to fit the potential energy data from the *ab initio* calculation in this work. The fitting equations can be expressed as

$$V(r) = G_2 \left(\sum_{i=1}^{m} w_{2i} f(w_{1i} G_1(r) + b_{1i}) + b_2 \right), \tag{7}$$

where f is the sigmoid activation function in this study, and G_1 and G_2 are normalized and denormalized functions, respectively. w_{1i} and b_{1i} are the corresponding weights and biases for neuron i, and w_{2i} and b_2 are the parameters for the output layer. The present NN model contains one hidden layer with m (= 10) neurons, which has been proved to be sufficient for atom-atom interactions. The root-mean-square errors (RMSEs) of the fitting PECs are below 0.005 eV for most molecular states, and they are around 0.05 eV for molecular states that contain irregular regions (due to the presence of avoided crossings and potential barriers). Apart from the NN model, the HH [21] and MS [22] analytical potential functions are also used for comparison in this work. The HH and MS functions can be expressed, respectively, as

$$V_{HH}(r) = D_e \Big(1 - \mathrm{e}^{-\alpha (r/r_{e-1})^2} + \beta (r/r_{e-1})^3 (1 + \gamma (r/r_{e-1})) \mathrm{e}^{-2\alpha (r/r_{e-1})} - 1 \Big), \tag{8}$$

$$V_{MS}(r) = -D_e (1 + a_0 + a_1 (r - r_e) + a_2 (r - r_e)^2 + a_3 (r - r_e)^3 + a_4 (r - r_e)^4) \mathrm{e}^{-a_5 (r - r_e)}, \tag{9}$$

where D_e and r_e are the potential well and equilibrium distance, respectively. α, β, γ and a_{0-5} are parameters to be fitted.

2.2. Ab initio calculations of PECs

In this study, the MOLPRO 2022 package [48, 49] is used for the *ab initio* calculations of PECs. All of the N–N and O–O PECs are calculated by the complete active space self-consistent field (CASSCF) method [50] followed by the valence internally contracted MRCI (icMRCI) [51, 52] approach with the Davidson correction [53]. In CASSCF, the state-averaged technique is employed for the electronic states with the same spin and symmetry. For extrapolating the potential energies to the complete basis set limit, the basis-set extrapolation method, the same as Qin *et al* [54, 55], is used in this work with aug-cc-pVQZ (AVQZ) and aug-cc-pV5Z (AV5Z) basis sets [56, 57]. The N_2 and O_2 molecules are homonuclear diatomic molecules, which have the $D_{\infty h}$ symmetry. The $D_{\infty h}$ symmetry is converted to D_{2h} symmetry for the calculation in MOLPRO 2022 package, which only allows Abelian point-group symmetries. Specifically, the above conversion results in the mapping of irreducible representations, i.e. $\Sigma_g^+ \rightarrow A_g$, $\Sigma_g^- \rightarrow B_{1g}$, $\Sigma_u^+ \rightarrow B_{1u}$, $\Sigma_u^- \rightarrow A_u$, $\Pi_g \rightarrow B_{2g} + B_{3g}$, $\Pi_u \rightarrow B_{2u} + B_{3u}$, $\Delta_g \rightarrow A_g + B_{1g}$, and $\Delta_u \rightarrow A_u + B_{1u}$. The electrons in the $2s2p$ shell of N and O atoms are placed in the active space, consisting of full valence space. In the calculation of N-N interactions, in addition to the valence molecular orbitals (MOs), one more σ_g and two more π_u MOs are included into the active space to better treat the Rydberg character of the electronic states [31, 32], especially for the higher-lying electronic states. For the O-O case, a similar treatment is applied. All of the calculated electronic states correlating to different dissociation limits of N_2 and O_2 are listed in table 1.

As will be seen in the *ab initio* results in section 3, the avoided crossings exist in the PECs of N_2 and O_2 which have same symmetry and spin [32, 58–61]. In principle, either the adiabatic or diabatic representation can be used to describe the PECs with avoided crossing. However, the adiabatic PECs have singularities near the crossing points [62], leading to lower fitting accuracy of the PECs and less numerical robustness in collision integral calculations. Moreover, based on the Landau–Zener method [63], an earlier calculation for nitrogen showed that the diabatic paths in collisions are much more likely to be followed than the adiabatic paths through the avoided crossing [58]. Therefore, in this paper, we calculate the diabatic PECs, based on which the collision integrals are evaluated. In general, the diabatic PECs are calculated by transforming the adiabatic representation into the diabatic representation [64]. For the two-state systems ($V^a{}_1$ and $V^a{}_2$ are the two adiabatic PECs), the transformation can be described by a unitary matrix U as [64]

$$V^d(R) = U^\dagger V^a(R) U = \begin{bmatrix} V_1^d(R) & V_{12}^d(R \\ V_{12}^d(R) & V_2^d(R) \end{bmatrix} = \begin{bmatrix} V_1^a \cos^2\theta + V_2^a \sin^2\theta & \frac{1}{2}(V_2^a - V_1^a)\sin(2\theta) \\ \frac{1}{2}(V_2^a - V_1^a)\sin(2\theta) & V_1^a \sin^2\theta + V_2^a \cos^2\theta \end{bmatrix}, \tag{10}$$

where the superscripts d and a refer to the diabatic and adiabatic bases, respectively, and θ is the nonadiabatic mixing angle which can be calculated by integrating the nonadiabatic coupling terms (NACTs) $\langle \Psi_i^{ad} | \partial / \partial R | \Psi_j^{ad} \rangle$ or the CI vector method [62, 65, 66]. In this work, the CI vectors method is used for the avoided crossings due to the two-state coupling. To be more specific, to implement the CI vector method, we use the quasi-diabatization procedure [67] implemented in MOLPRO 2022 package, and the symmetry is reduced from $D_{\infty h}$ to C_{2v} in the diabatic calculations. In contrast,

Table 1. Valence states of N_2 and O_2 and their dissociation limits.

Dissociation limit	Molecular states				
N(^{4}S)-N(^{4}S)	$X^1\Sigma_g^+$	$A^3\Sigma_u^+$	$A'^5\Sigma_g^+$	$1^7\Sigma_u^+$	
N(^{2}D)-N(^{4}S)	$B^3\Pi_g$	$W^3\Delta_u$	$C^3\Pi_u$	$G^3\Delta_g$	$E^3\Sigma_g^+$
	$2^3\Sigma_u^+$	$C'^5\Pi_u$	$2^5\Sigma_g^+$	$1^5\Pi_g$	$1^5\Delta_g$
	$1^5\Delta_u$	$1^5\Sigma_u^+$			
N(^{2}P)-N(^{4}S)	$B'^3\Sigma_u^-$	$1^3\Sigma_g^-$	$2^3\Pi_u$	$2^3\Pi_g$	
	$2^5\Pi_u$	$1^5\Sigma_g^-$	$2^5\Pi_g$	$2^5\Sigma_u^-$	
O(^{3}P)-O(^{3}P)	$X^3\Sigma_g^-$	$(b,2)^1\Sigma_g^+$	$c^1\Sigma_u^-$	$1^1\Pi_g$	$1^1\Pi_u$
	$a^1\Delta_g$	$(A,2)^3\Sigma_u^+$	$1^3\Pi_g$	$1^3\Pi_u$	$C^3\Delta_u$
	$(1,2)^5\Sigma_g^+$	$^5\Sigma_u^-$	$1^5\Pi_g$	$1^5\Pi_u$	$^5\Delta_g$
O(^{3}P)-O(^{1}D)	$^3\Sigma_g^+$	$(2,3)^3\Sigma_g^-$	$3^3\Sigma_u^+$	$(B,2)^3\Sigma_u^-$	$1^3\Phi_g$
	$(2,3,4)^3\Pi_g$	$(2,3,4)^3\Pi_u$	$(1,2)^3\Delta_g$	$(2,3)^3\Delta_u$	$1^3\Phi_u$
O(^{1}D)-O(^{1}D)	$(3,4,5)^1\Sigma_g^+$	$(2,3)^1\Sigma_u^-$	$(2,3)^1\Pi_g$	$(2,3)^1\Pi_u$	$(2,3)^1\Delta_g$
	$1^1\Delta_u$	$1^1\Phi_g$	$1^1\Phi_u$	$1^1\Gamma_g$	
O(^{3}P)-O(^{1}S)	$4^3\Sigma_g^-$	$3^3\Sigma_u^-$	$5^3\Pi_g$	$5^3\Pi_u$	
O(^{1}D)-O(^{1}S)	$6^1\Sigma_g^+$	$1^1\Sigma_u^+$	$4^1\Pi_g$	$4^1\Pi_u$	$4^1\Delta_g$
	$2^1\Delta_u$				
O(^{1}S)-O(^{1}S)	$7^1\Sigma_g^+$				

for the multiple-states coupling cases, we either reduce the configuration spaces to decrease the number of crossings and obtain diabatic PECs [67] or simply interchange the adiabatic points [58]. In addition, for each state where an avoided crossing occurs, we calculate three higher excited states that share the same symmetry and spin characteristics. In most cases within the N–N system, the first five states are computed for the symmetry featuring an avoided crossing. For the O–O system, we extend our calculations to encompass the first seven states.

3. Results and discussion

3.1. PECs based on ab initio calculations

3.1.1. PECs of N_2. The present PECs of N_2 in the diabatic representation are shown in figure 1. The results of Qin *et al* [33, 34] in the adiabatic representation are also shown for comparison and good agreements are achieved for most of the states. However, for the $1^7\Sigma_u^+$, $2^5\Sigma_g^+$, and $2^3\Pi_g$ states, the differences are found in the short range where the present energies are smaller. It is noted that the results of Qin *et al* [33, 34] in the short range for these states were obtained by extrapolation. Besides, for the $E^3\Sigma_g^+$, $C^3\Pi_u$, $2^3\Pi_u$, $1^5\Sigma_u^+$, $1^5\Delta_u$ and $2^5\Sigma_u^-$ states, avoided crossings occur in these states so significant differences are found between the present PECs and those of Qin *et al* [33, 34], with the latter showing unsmooth behavior near the avoided crossings. Specifically, for the $C^3\Pi_u$ state, avoided crossing is found at 2.59 a.u. of N_2 bond distance, which is consistent with the one reported in references [32, 58]. This crossing point is below the dissociation limit, and the coupling energy is 0.1025 eV. For the $2^3\Pi_u$ state, avoided crossing occurs at 3.90 a.u. and is higher than the dissociation limit, with the coupling energy being 0.0056 eV. For the $E^3\Sigma_g^+$, $1^5\Sigma_u^+$, $1^5\Delta_u$ and $2^5\Sigma_u^-$ states, avoided crossings occur at 3.44 a.u., 3.05 a.u., 2.90 a.u., and 2.98 a.u., respectively, and the coupling energies are 0.042 eV, 0.075 eV, 0.049 eV, and 0.050 eV, respectively. To describe the avoided crossings more clearly, the adiabatic PECs, diabatic PECs, and NACTs for avoided crossings are shown in figure 2. It shows that the non-zero NACTs are found at the crossings, and the diabatic representations of the PECs (dashed lines) are smoothed through the matrix transformation in equation (10).

Table 2 presents the potential wells, equilibrium distances, and vertical excitation energies of selected N_2 electronic states, compared to the available experimental data [68–70]. For the $X^1\Sigma_g^+$ and $A^3\Sigma_u^+$ states relating to the N(^4S)-N(^4S) dissociation limit, the differences of the potential wells D_e between the present calculation and the experimental data [68] are 0.007 eV and 0.013 eV, respectively. For the $B^3\Pi_g$, $W^3\Delta_u$, and $C^3\Pi_u$ states relating to the dissociation limit of N(^4S)-N(^2D) as well as $B'^3\Sigma_u^-$ associated to N(^4S)-N(^2P), the differences of D_e are all smaller than 0.02 eV compared to the experimental data [68]. The differences between the calculated equilibrium distance R_e and the experimental value are all below 0.01 Å. Moreover, the differences of vertical excitation energies E_{ve} (excitation energies from the $X^1\Sigma_g^+$ electronic ground state) are smaller than 0.05 eV for all excited states compared to the experimental data [69]. It is noted that this is a better agreement than the result in [70] where the cc-pVQZ basis set is employed. Furthermore, the calculated energy separation between N(^4S) and N(^2D) is 2.392 eV and that between N(^4S) and N(^2P) is 3.589 eV while the experimental data are found to be 2.383 eV and 3.575 eV, respectively [68, 71]. All the above comparisons suggest the reliability of the present *ab initio* results.

We then use the MS, HH, and NN potential energy functions to fit the *ab initio* points to PECs. The fitting accuracies of the above three formulas are compared in figure 3 for the typical states, i.e. $X^1\Sigma_g^+$, $A'^5\Sigma_g^+$, and $2^3\Sigma_u^+$ states, with the last one having a potential barrier. For the $X^1\Sigma_g^+$ state, the RMSEs of the NN, MS, and HH PECs are 0.0005 eV, 0.2021 eV, and

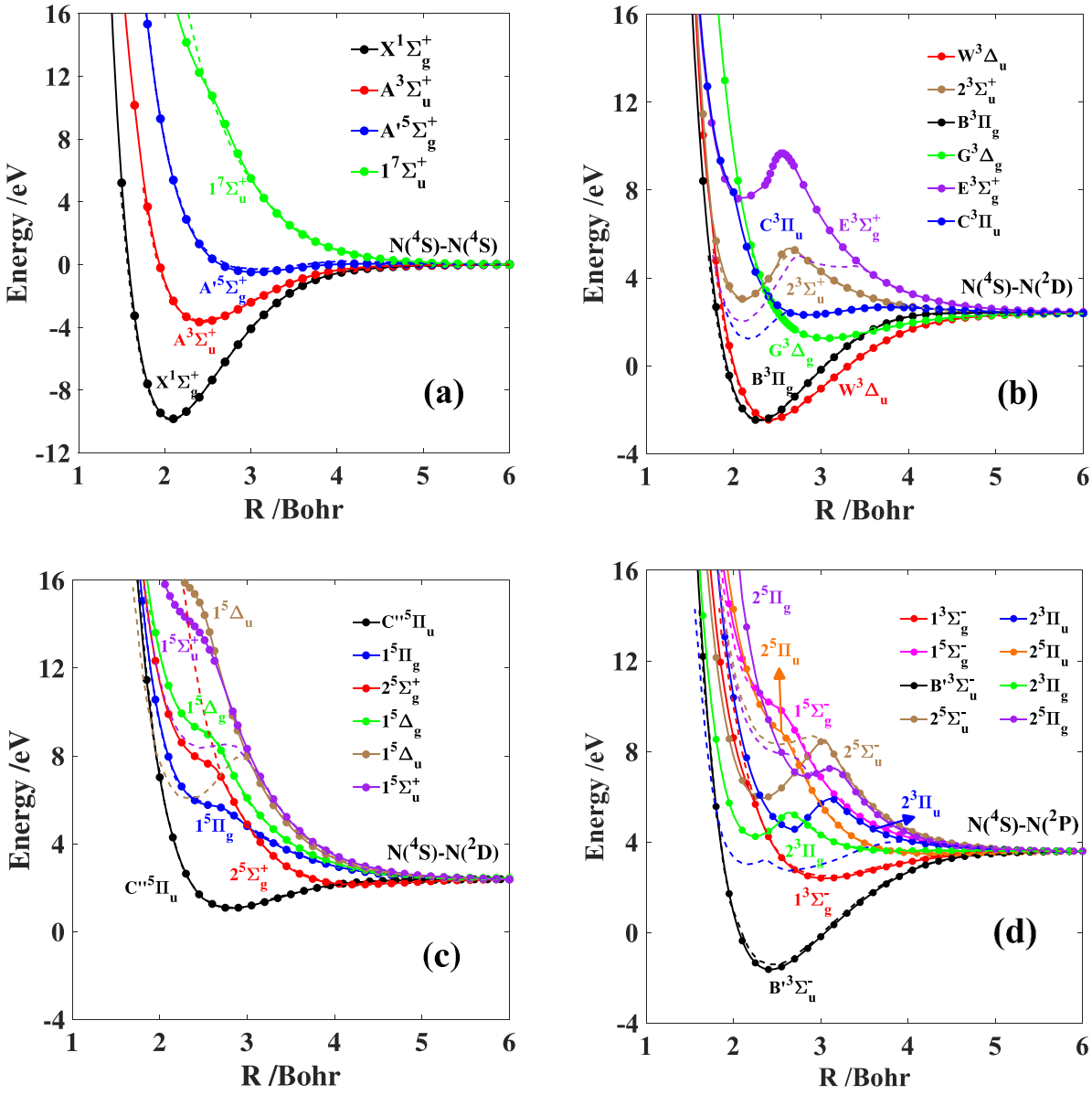

Figure 1. The PECs of N_2. The solid lines are the results of this work in the diabatic representation, and the dotted lines are the results of Ding *et al* [34] in the adiabatic representation. (a) The states corresponding to N(^{4}S)-N(^{4}S). (b) The triplet states corresponding to N(^{4}S)–N(^{2}D). (c) The quintet states corresponding to N(^{4}S)–N(^{2}D). (d) The states corresponding to N(^{4}S)–N(^{2}P).

0.2529 eV, respectively. Moreover, the RMSE of NN, MS, and HH PECs are 0.0091 eV, 0.0867 eV, and 0.0963 eV for the $A'^5\Sigma_g^+$ state, and 0.0542 eV, 0.2655 eV, and 0.2981 eV for the $2^3\Sigma_u^+$ state. Specifically, for the $2^3\Sigma_u^+$ state, significant differences can be seen near the barrier region for the MS and HH PECs, while the NN PEC performs well and its deviation from the *ab initio* data is below 0.1 eV in this region. Overall, the NN PECs have much higher accuracy than the MS and HH PECs.

3.1.2. PECs of O_2. The present PECs for the O(^3P)–O(^3P), O(^3P)–O(^1D), O(^1D)–O(^1D), and O(^1S)–O(^3P,^1D,^1S) interactions in the diabatic representation are shown in figures 4–8, respectively. Good agreements are found between the present PECs and those in adiabatic representation developed by Liu *et al* [29], with the current *ab initio* data being extended to the shorter range and covering the energy range of −6 − 15 eV. For the O(^3P)-O(^3P) interaction, the avoided crossings are found at 3.10 a.u., 3.55 a.u., 3.00 a.u., and 3.20 a.u. for the $2^1\Sigma_g^+$, $2^3\Sigma_u^+$, $1^1\Pi_g$, and $1^3\Pi_g$ states, respectively, with the coupling energies being 0.041 eV, 0.033 eV, 0.0457 eV, and 0.056 eV, respectively. For these avoided crossings, the adiabatic PECs, diabatic PECs, and NACTs are shown in figure 5. It also shows that the NACTs are non-zero at the crossings, and the diabatic representations of the PECs (dashed lines) are smoothed through diabatization procedure. The avoided crossings occurring in the $1^1\Pi_g$ and $1^3\Pi_g$ are also found to be about 3.00 a.u. in [10]. Moreover, it is also seen in figures 4–8 that the avoided crossings exist in the PECs of the $2^3\Delta_u$ and $3^3\Sigma_u^+$

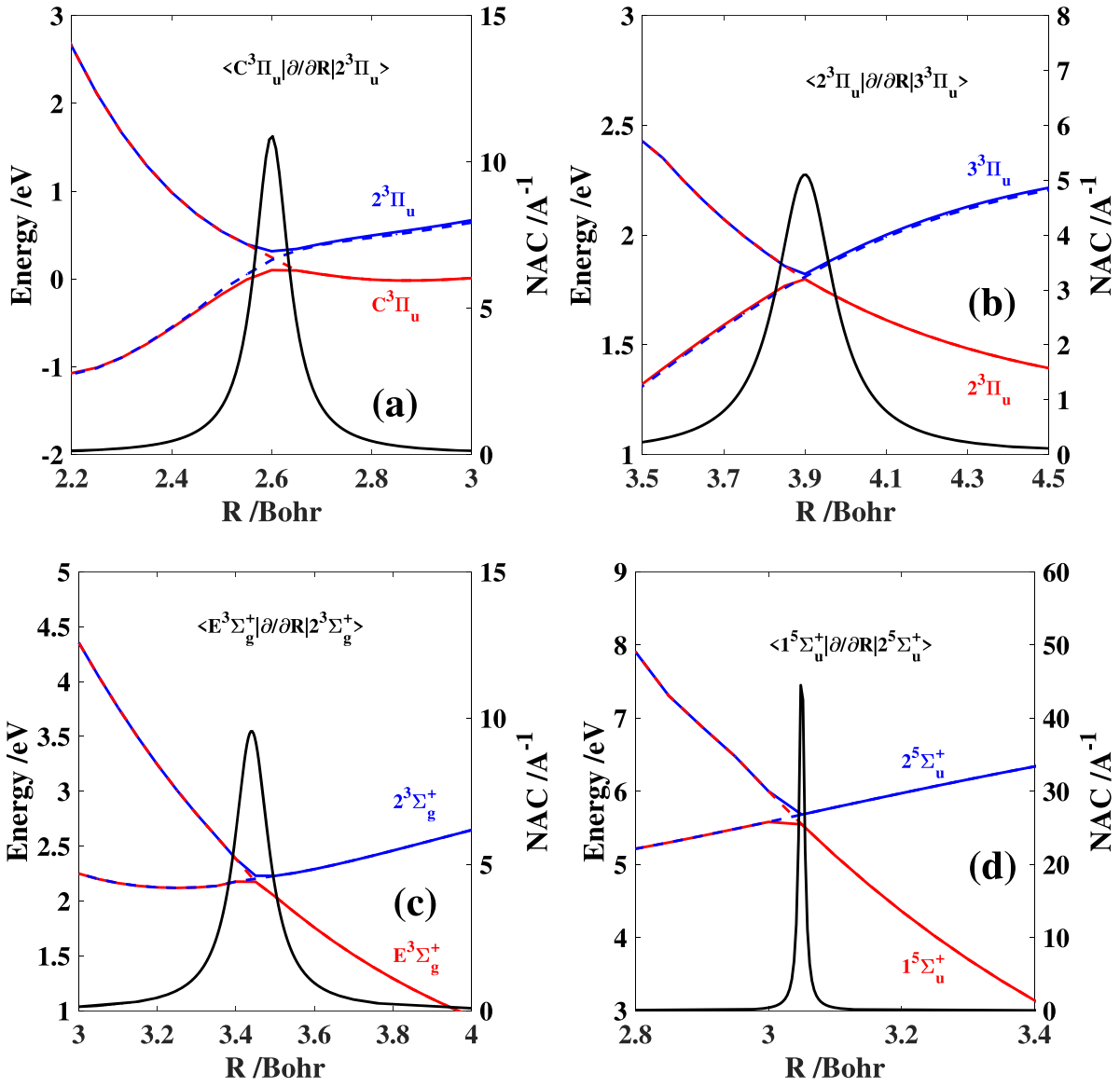

Figure 2. Illustration of avoided crossings in the N-N system. The red and blue solid lines are the adiabatic PECs, the dotted lines are the diabatic PECs, and the black solid lines correspond to the nonadiabatic coupling terms. (a) Avoided crossing between $C^3\Pi_u$ and $2^3\Pi_u$. (b) Avoided crossing between $2^3\Pi_u$ and $3^3\Pi_u$. (c) Avoided crossing between $E^3\Sigma_g^+$ and $2^3\Sigma_g^+$. (d) Avoided crossing between $1^5\Sigma_u^+$ and $2^5\Sigma_u^+$.

Table 2. The potential wells D_e (in eV), equilibrium distances R_e (in Å), and vertical excitation energies E_{ve} (in eV) at equilibrium bond length $R = 1.0977$ Å of N_2 electronic states.

State	D_e(Present)	D_e(Expt.)	R_e(Present)	R_e(Expt.)	E_{ve}(Present)	E_{ve}(Expt.)
$X^1\Sigma_g^+$	9.912	9.905[a]	1.0980	1.0977[a]		
$A^3\Sigma_u^+$	3.693	3.680[a]	1.2965	1.2866[a]	7.79	7.75[b]
$B^3\Pi_g$	4.878	4.896[a]	1.2171	1.2126[a]	8.08	8.04[b]
$W^3\Delta_u$	4.865	4.873[a]	1.2806	1.2796[a]	8.91	8.88[b]
$B'^3\Sigma_u^-$	5.260	5.264[a]	1.2806	1.2784[a]	9.72	9.67[b]
$C^3\Pi_u$	1.250	1.237[a]	1.1483	1.1487[a]	11.20	11.19 [b]

[a] Lofthus and Krupenie [68].
[b] Oddershede *et al* [69].

states for the O(^3P)–O(^1D) interaction, of the $2^1\Delta_g$, $3^1\Sigma_g^+$, $4^1\Sigma_g^+$, $5^1\Sigma_g^+$, and $1^1\Gamma_g$ for the O(^1D)–O(^1D) interaction, and of the $6^1\Sigma_g^+$ state for the O(^1D)-O(^1S) interaction.

Table 3 reports the potential well depths D_e and equilibrium distances R_e for the selected states of the O(^3P)–O(^3P) interaction The available experimental data [72, 73] and numerical

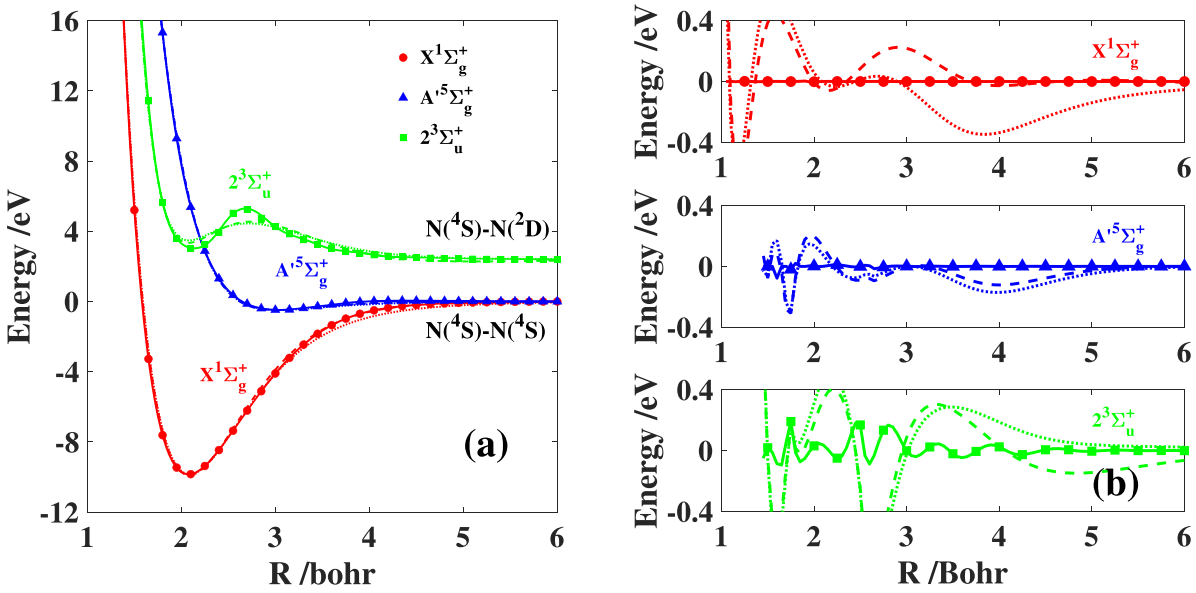

Figure 3. The PECs for the $X^1\Sigma_g^+$ (circles), $A'^5\Sigma_g^+$ (triangles), and $2^3\Sigma_u^+$ (squares) states of the N–N system. (a) The comparison of the NN (solid lines), MS (dashed lines), and HH (dotted lines) PECs. (b) The deviation between the present *ab initio* data and the fitting PECs.

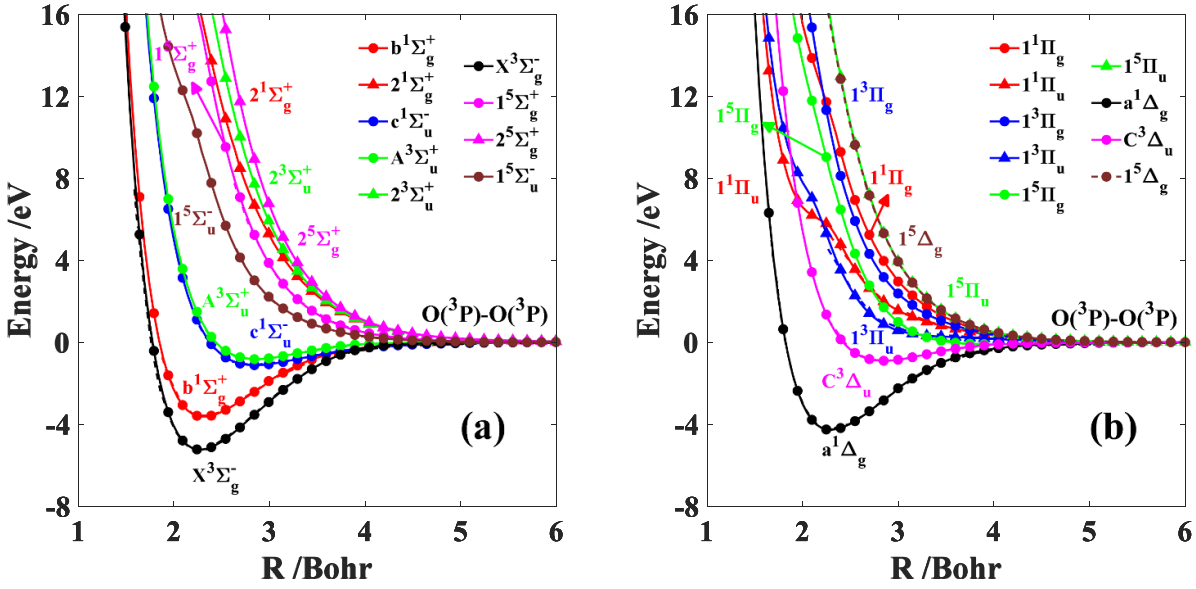

Figure 4. The PECs of the O(^3P)–O(^3P) interactions. The solid lines are the results of this work in the diabatic representation, and the dotted lines are the results of Liu *et al* [29] in the adiabatic representation. (a) The PECs of the Σ states. (b) The PECs of the Π and Δ states.

results by Saxon *et al* [74] are also included for comparison. It can be seen that the difference of D_e is 0.009 eV between the present values and the experimental data [73] for the ground state $X^3\Sigma_g^-$, and this agreement is much better than the results of Saxon *et al* [74]. The high accuracy of present calculation is also found for the equilibrium distance R_e, with a difference of only 0.004 Å compared to the experimental data [73]. For the $c^1\Sigma_u^-$, $C^3\Delta_u$, and $A^3\Sigma_u^+$ states, compared to the available experimental data [72], the differences are less than 0.003 eV for D_e and 0.01 Å for R_e. For the $a^1\Delta_g$ and $b^1\Sigma_g^+$ states, the differences are slightly larger than 0.025 eV and 0.039 eV for D_e. Furthermore, in the present *ab initio* calculations, the energy separations between O(^3P) and O(^1D) (or O(^1S)) is 1.953 eV (or 4.156 eV), which agrees well with the experimental data [75, 76] of 1.967 eV (or 4.190 eV). All the above comparisons suggest the reliability of the present *ab initio* results of O_2.

By adopting the aforementioned MS, HH, and NN potential energy functions, we also fit the *ab initio* points to the PECs of O_2. The fitting accuracy for the above functions is shown in figure 9, in which the results of the piecewise fitting curves of Levin *et al* [7] and the exponential and Mores form PECs developed by Laricchiuta *et al* [37] are also compared. In figures 9(a) and (b), the NN PECs (solid lines) are first compared to the PECs developed by Levin *et al* [7] (dashed lines) and Laricchiuta *et al* [37] (dotted lines) for the

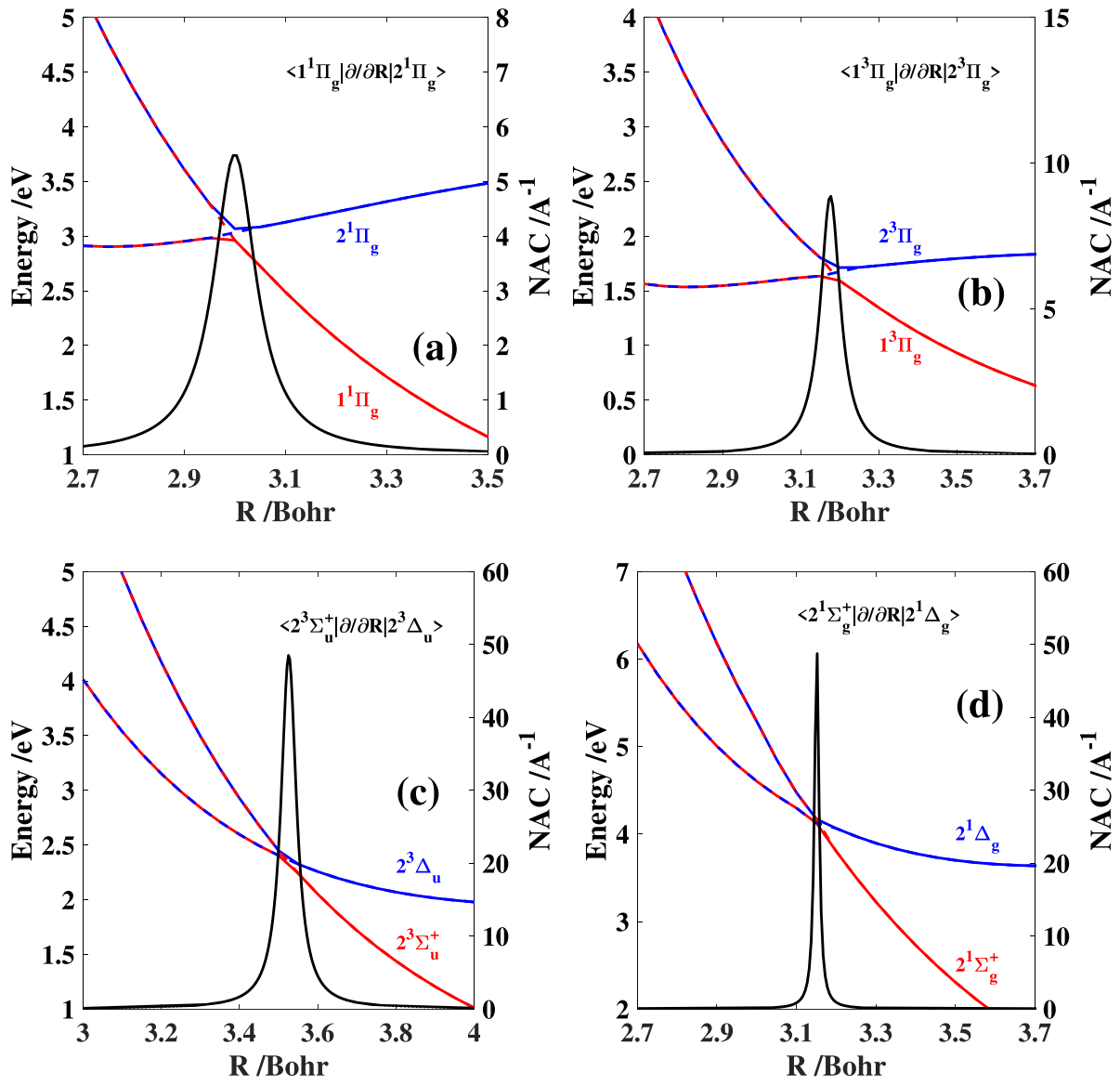

Figure 5. Illustration of avoided crossings for O(^3P)–O(^3P) interactions. The red and blue solid lines are the adiabatic PECs, the dotted lines are the diabatic PECs, and the black solid lines correspond to the nonadiabatic coupling terms. (a) Avoided crossing between $1^1\Pi_g$ and $2^1\Pi_g$. (b) Avoided crossing between $1^3\Pi_g$ and $2^3\Pi_g$. (c) Avoided crossing between $2^3\Sigma_u^+$ and $2^3\Delta_u$. (d) Avoided crossing between $2^1\Sigma_g^+$ and $2^1\Delta_g$.

$X^3\Sigma_g^-$, $C^3\Delta_u$, and $^1\Pi_u$ states. It is seen that the present NN PECs are overall very well-fitted to the *ab initio* data compared to the other curves. The RMSEs of Levin's PECs with respect to the NN PECs are 0.2537 eV, 0.6837 eV and 0.1146 eV for the $X^3\Sigma_g^-$, $^1\Pi_u$ and $C^3\Delta_u$ states, respectively, while those of Laricchiuta's PECs are 0.8743 eV, 1.2670 eV and 0.3691 eV. So, for the PECs of the $X^3\Sigma_g^-$ and $C^3\Delta_u$ states, the PECs by Levin *et al* [7] are closer to the *ab initio* data and the NN PECs, since the authors [7] combined the spectroscopic and other experimental data and theoretical *ab initio* data to construct the PECs. However, for the $^1\Pi_u$ state, the PECs of Levin *et al* [7] and Laricchiuta *et al* [37] are close to each other, but both of them deviate significantly from the present high-accuracy *ab initio* data in the repulsive region. The reason is likely to be that the PECs of Levin and Laricchiuta were fitted to the low-level *ab initio* data obtained using fewer configuration state functions and basis sets as the computing resources were limited at that time [74]. The fitting accuracy of NN (solid lines) is then compared to the MS (dashed lines) and HH (dotted lines) PECs in figures 9(c) and (d). For the $X^3\Sigma_g^-$ state, the RMSE of NN, MS, and HH PECs are 0.0001 eV, 0.1291 eV, and 0.2251 eV, respectively. For the $^1\Pi_u$ (and $C^3\Delta_u$) states, the RMSE of NN, MS, and HH PECs are 0.0118 eV, 0.1567 eV, and 0.1705 eV (0.0010 eV, 0.0280 eV, and 0.0454 eV), respectively.

In summary, the results of the O–O as well as N–N systems above have demonstrated the extremely high accuracy of the NN PECs in fitting the *ab initio* calculation data.

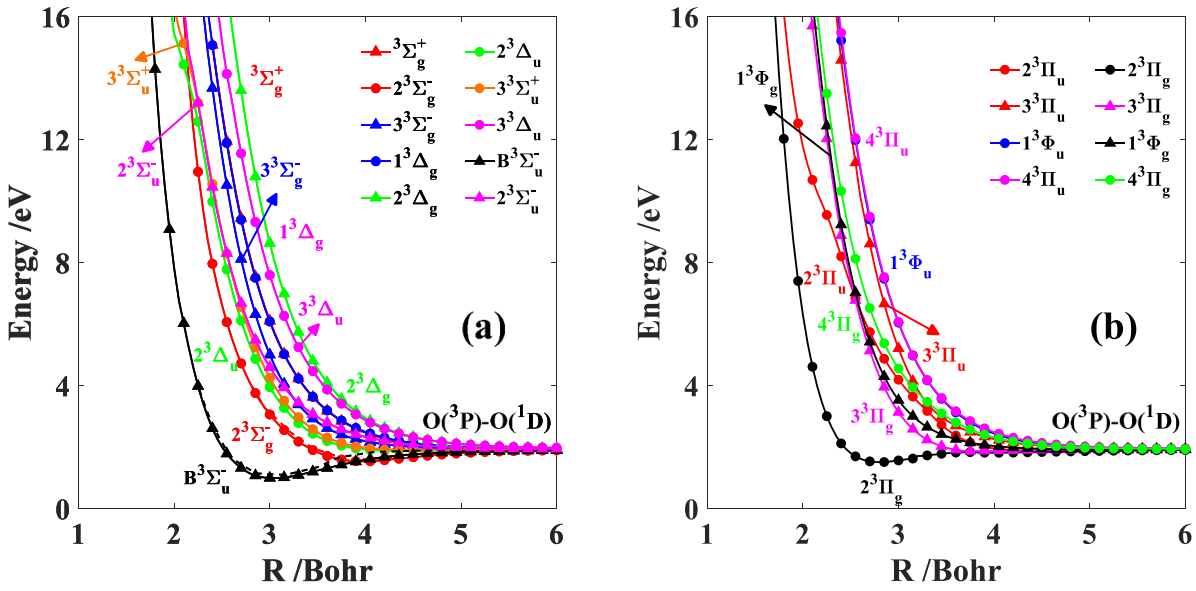

Figure 6. The PECs of the O(^3P)–O(^1D) interactions. The solid lines are the results of this work in the diabatic representation, and the dotted lines are the results of Liu *et al* [29] in the adiabatic representation. (a) The PECs of the Σ and Δ states. (b) The PECs of the Π and Φ states.

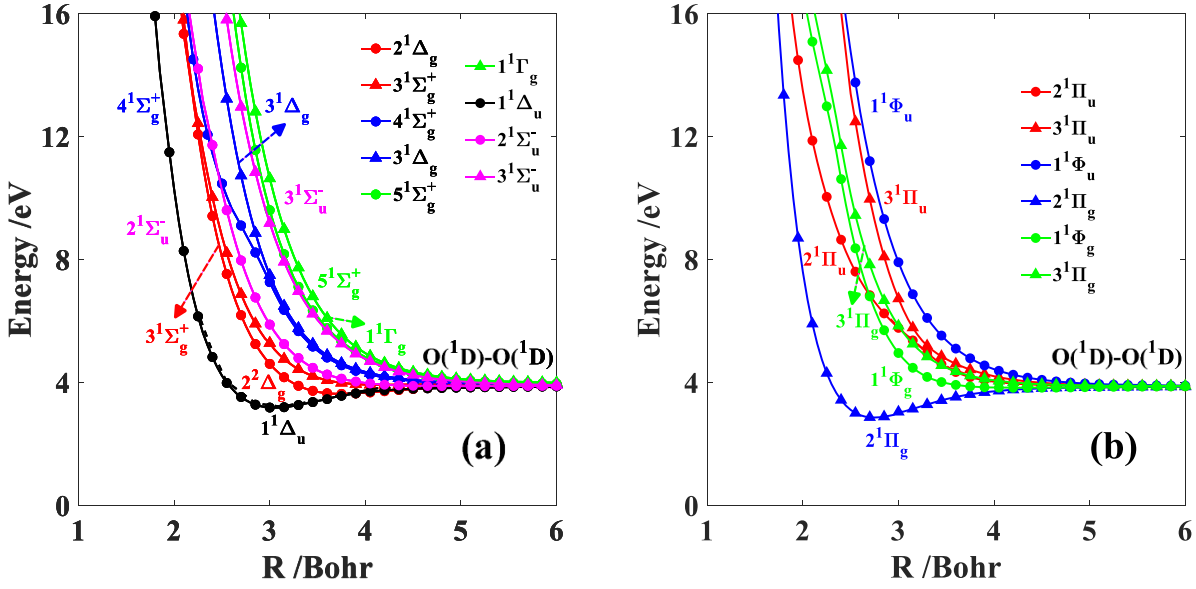

Figure 7. The PECs of the O(^1D)–O(^1D) interactions. The solid lines are the results of this work in the diabatic representation, and the dotted lines are the results of Liu *et al* [29] in the adiabatic representation. (a) The PECs of the Σ and Δ states. (b) The PECs of the Π and Φ states.

3.1.3. Nonadiabatic transitions at crossings and avoided crossings. For the crossings and avoided crossings in the N–N and O–O PECs, it is interesting to evaluate the nonadiabatic transition probabilities and examine the rationality of using the diabatic PECs in this paper. The Zhu–Nakamura theory [77, 78] is used in this work for both crossings and avoided crossings, which are further divided into two categories [77–79], i.e. the crossing curves with the same (Landau–Zener case, LZ) and different (Nonadiabatic Tunneling case, NT) sign slopes. Only the contributions coming from the colliding particles having kinetic energy E larger than the potential energy E_x at the crossing point in the LZ case [78, 79] and larger than the upper adiabatic potential energy E_b in the NT case [77] need to be considered. Specifically, in the LZ case, the nonadiabatic transition probability for one passage of avoided crossing point (or the survival probability for one passage of crossing point) p can be expressed as [78]

$$p = \exp\left[-\frac{\pi}{4a}\left(\frac{2}{b^2+\sqrt{b^4+0.4a^2+0.7}}\right)^{1/2}\right] \qquad (11)$$

with

$$a^2 = \frac{\hbar^2}{2m}\frac{F(F_1-F_2)}{8V_x^3} \geqslant 0, b^2 = (E-E_x)\frac{F_1-F_2}{2FV_x}, \qquad (12)$$

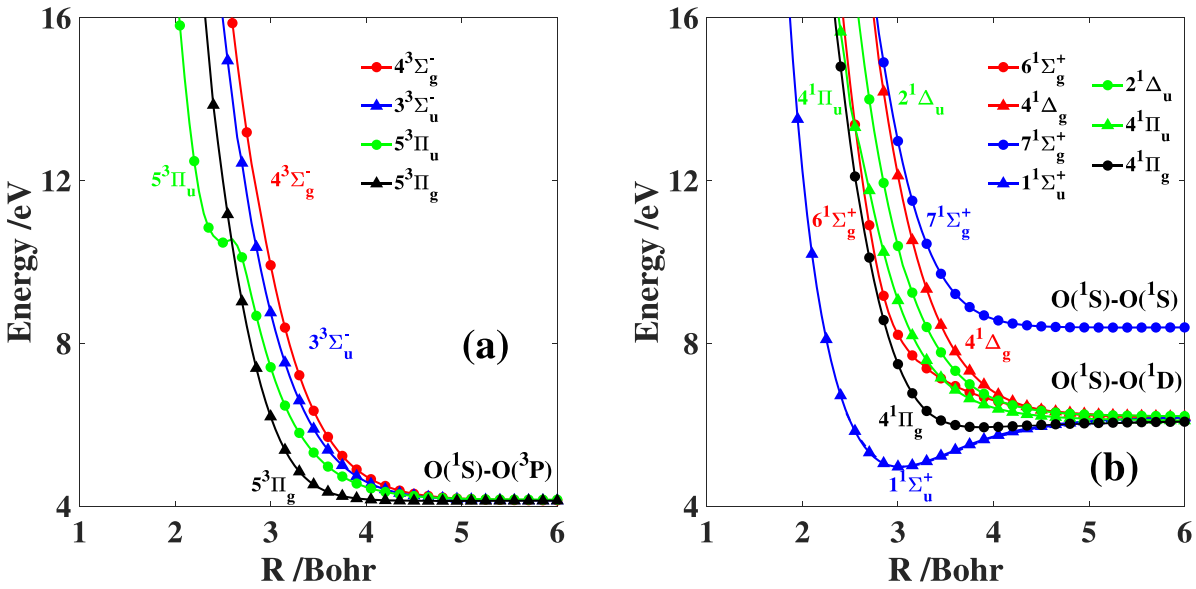

Figure 8. The PECs of the O(^1S)–O(^3P,^1D,^1S) interactions. The solid lines are the results of this work in the diabatic representation, and the dotted lines are the results of Liu *et al* [29] in the adiabatic representation. (a) The PECs for the O(^1S)–O(^3P) interactions. (b) The PECs for the O(^1S)–O(^1D,^1S) interactions.

Table 3. The potential well depths D_e (in eV) and equilibrium bond lengths R_e (in Å) of the present PECs, and the available experimental data [72, 73] and the calculated data of Saxon *et al* [74] are also given.

State	D_e (Saxon)	D_e (Present)	D_e (Expt.)	R_e (Saxon)	R_e (Present)	R_e (Expt.)
$X^3\Sigma_g^-$	4.957[a]	5.222	5.213[b]	1.236[a]	1.204	1.208[b]
$a^1\Delta_g$	3.857[a]	4.257	4.232[c]	1.250[a]	1.217	1.216[c]
$b^1\Sigma_g^+$	3.168[a]	3.616	3.577[c]	1.267[a]	1.230	1.227[c]
$c^1\Sigma_u^-$	1.062[a]	1.116	1.114[c]	1.555[a]	1.508	1.517[c]
$C^3\Delta_u$	0.825[a]	0.904	0.907[c]	1.550[a]	1.508	
$A^3\Sigma_u^+$	0.745[a]	0.826	0.824[c]	1.558[a]	1.521	1.521[c]

[a] Saxon *et al* [74].
[b] Herzberg *et al* [73].
[c] Krupenie *et al* [72].

$$F_i = \mathrm{d}V_i^d(r_x)/\mathrm{d}r - \frac{\hbar^2}{2m}\frac{(l+1)\,l}{r_x^3}, \qquad (13)$$

where E is the kinetic energy of colliding particles, V_x is the coupling energy of the two crossing PECs (V_1^d and V_2^d) at crossing point r_x, F is $\sqrt{|F_1F_2|}$, l is the orbital angular momentum quantum number, and m is the reduced mass of colliding particles. In the NT case, the probability p can be expressed as [77]

$$p = \exp\left[-\frac{\pi}{4a}\left(\frac{2}{b^2+\sqrt{b^4+0.62a^{1.43}-0.72}}\right)^{1/2}\right], \qquad (14)$$

where the definitions of a and b are given in equation (12).

Figure 10 shows the crossing (marker 1) between the $B^3\Pi_g$ and $W^3\Delta_u$ states of the N-N system and the avoided crossing (marker 2) between the $1^3\Pi_g$ and $2^3\Pi_g$ states in adiabatic representations of the O–O system. For crossing 1, the coupling energy V_x is set to 100 cm^{-1} (a high coupling constant for low-mass atoms like nitrogen, compared to the metals) in calculating the survival probability. This yields $a^2 > 100$ and p larger than 99%, indicating the colliding particles take the adiabatic path at the crossing point. Furthermore, the survival probabilities p (V_x chosen to be 100 cm^{-1}) are all larger than 95% for the crossings of the N–N and O–O PECs, except for the crossing between the $2^3\Pi_g$ and $2^5\Pi_u$ PECs, which gives $p \approx 80\%$ due to the small $F_1 - F_2$. Therefore, the contribution of the nonadiabatic effects can be negligible for the present PEC crossings in the following collision integral calculations.

For the avoided crossing 2 in figure 10, the coupling energy is 0.056 eV, which gives intermediate coupling ($a^2 < 5$) and nonadiabatic transition probability p lagger than 90% when $E > 2.0$ eV. Accordingly, the colliding particles prefer the nonadiabatic path at the avoided crossing point. Moreover, the nonadiabatic transition probabilities p are more than 90% for the avoided crossings of the N–N and O–O PECs, except for the one occurring between the $C^3\Pi_u$ and $2^3\Pi_u$ PECs of the N–N system, which gives $p \approx 60\%$ when $E = 1.0$ eV due to the largest coupling energy of 0.1025 eV. Therefore, the analysis made above suggests that the diabatic PECs are much more likely to be followed for the avoided crossings encountered in the present N–N and O–O interactions. This justifies the

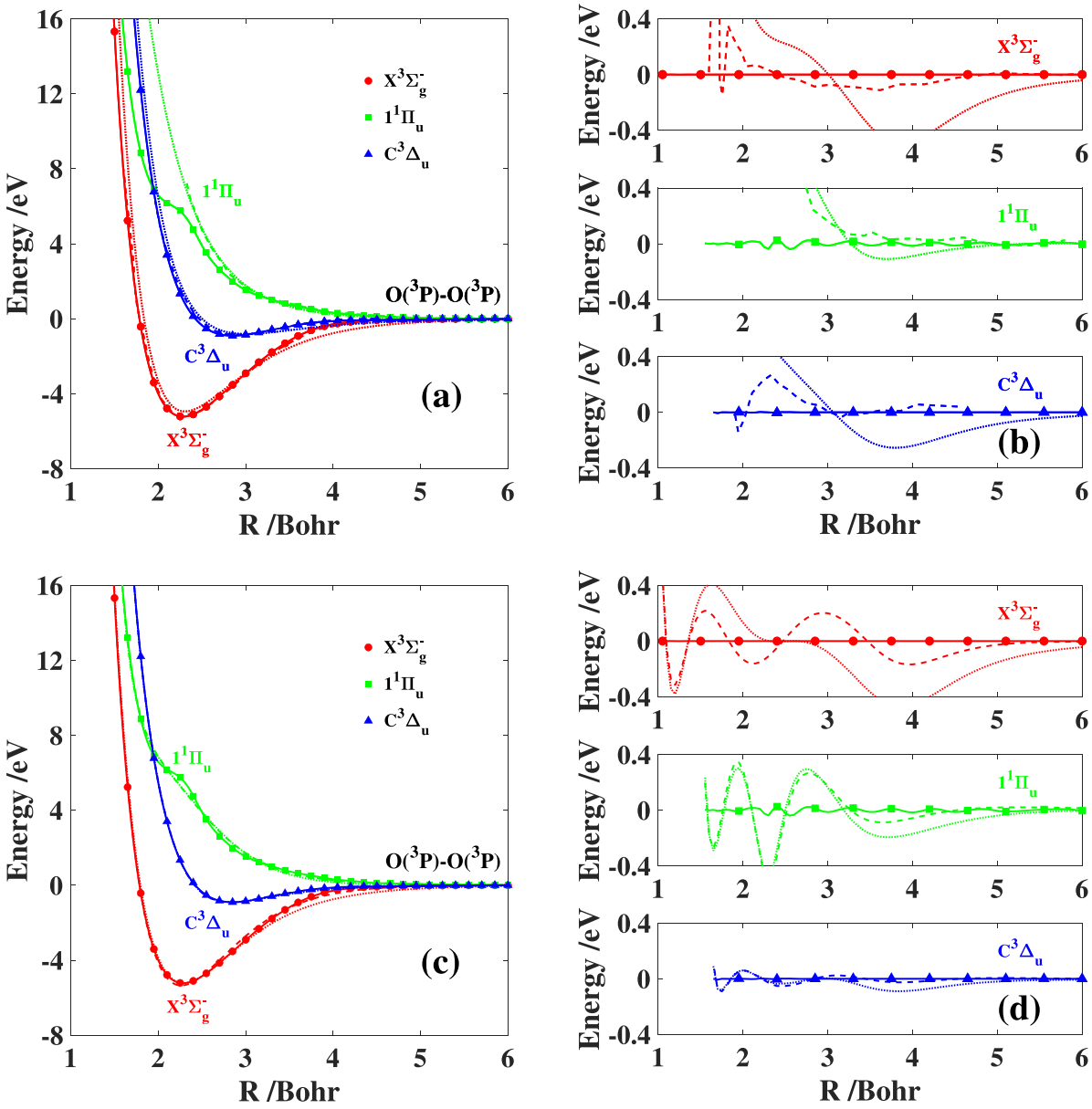

Figure 9. The PECs for the $X^3\Sigma_g^-$ (circles), $C^3\Delta_u$ (triangles), and $^1\Pi_u$ (squares) states of the O–O system. (a) The comparison of the NN PECs (solid lines) and PECs of Levin *et al* [7] (dashed lines) and of Laricchiuta *et al* [37] (dotted lines). (b) The deviation between different PECs and the present *ab initio* data. (c) The comparison of the NN (solid lines), MS (dashed lines), and HH (dotted lines) PECs. (d) The deviation between the fitting PECs and present *ab initio* data.

choice of diabatic PECs to calculate the collision integral in this work. Moreover, our argument is consistent with the discussion of Guberman [58].

3.2. Discussion of collision integrals

The present diffusion collision integrals $\sigma^2\Omega^{(1,1)*}$ have considered the inelastic contribution of resonant excitation processes. Therefore, we first examine the present program for calculating the inelastic contribution by comparing the results with the ones of Laricchiuta *et al* [37] for the O–O system. The same form and parameters of the PECs, given in [37], for the O(^3P)–O(^3P) and O(^3P)–O(^1D) interactions are adopted, and the results of $\sigma^2\Omega^{(1,1)*}$ (involving elastic and inelastic contributions) are shown in table 4. It is seen that the present results are in good agreement with the values reported by Laricchiuta *et al* [37], and the relative error is below 1% for the temperature of 2000 − 20 000 K.

Next, we test the impact of the PEC fitting accuracy on the collision integrals. By using the MS, HH, and NN PECs fitted in section 3.1, the viscous collision integrals $\sigma^2\Omega^{(2,2)*}$ of the $X^1\Sigma_g^+$, $A'^5\Sigma_g^+$, and $2^3\Sigma_u^+$ states of the N–N system (see figure 3 for the fitting details) and the $X^3\Sigma_g^-$, $C^3\Delta_u$, and $^1\Pi_u$ states of the O–O system (see figure 9 for the fitting details), and the results are shown in table 5. For the $X^1\Sigma_g^+$ state of N_2, the differences of $\sigma^2\Omega^{(2,2)*}$ between the MS and NN PECs are around 7% (500 K) at low temperatures and become smaller as the temperature increases. In contrast, the results of the

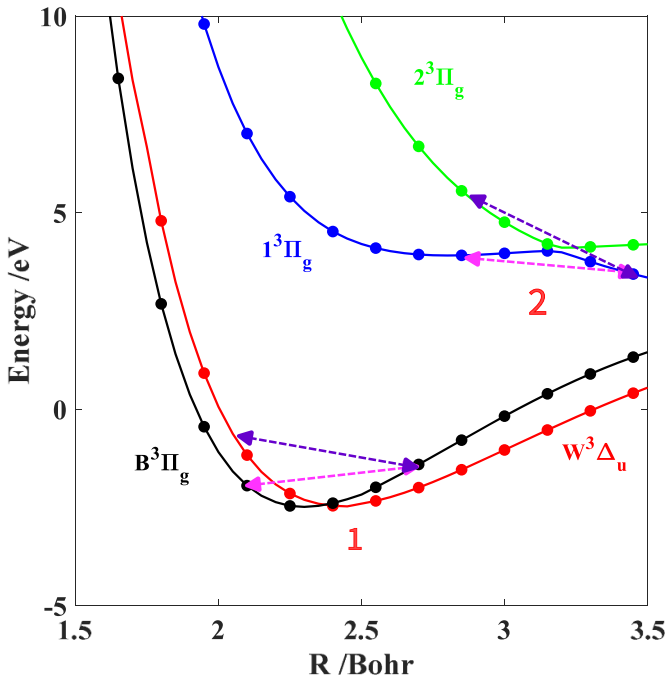

Figure 10. The crossing (1) between the $B^3\Pi_g$ and $W^3\Delta_u$ states in the N–N system, and the avoided crossing (2) between the $1^3\Pi_g$ and $2^3\Pi_g$ states in adiabatic representations of the O–O system. The pink arrow denotes the adiabatic path and the purple arrow denotes the nonadiabatic path.

HH PEC significantly differ from the MS and NN PECs, with more than 20% differences for T less than 5000 K. The reason for the significant differences can be inferred from figure 3 that the HH curve does not fit well the *ab initio* data in the long-range region, which is essential for calculating the collision integrals at low temperatures. A similar situation happens for the $A'^5\Sigma_g^+$ of N_2 with slightly larger differences between the MS and NN PECs for T less than 5000 K. However, for the $2^3\Sigma_u^+$ state of N_2, the results of both HH and MS PECs noticeably deviate from the NN ones for all the reported temperatures; the reason for this can also be inferred from figure 3 that the HH and MS functions both have significant fitting errors for the $2^3\Sigma_u^+$ state, which exhibits a barrier before potential well. Therefore, it is evident that the fitting accuracy of PECs dramatically influences the results of collision integrals, especially at lower temperatures.

In addition, for the $X^3\Sigma_g^-$ state of O_2, the results of the HH PEC again differ significantly from those of the MS and NN PECs, with more than 30% differences for T less than 5000 K. The big differences are explained by figure 9 that the long-range behavior of the HH PEC is poor. Overall, the HH formulation performs worse than the MS one in fitting the *ab initio* data of O_2 since the former has fewer fitting parameters. For the $C^3\Delta_u$ and $^1\Pi_u$ states of O_2, the results of $\sigma^2\Omega^{(2,2)*}$ calculated based on the MS PECs are close to those from the NN PECs, with a error of 5% at most at low temperatures because of the high fitting accuracy for both models. Furthermore, it is noted from the results above that the collision integrals are less sensitive to the exact shape of PEC at high temperatures, which was also pointed out in [28].

In summary, the high-accuracy fitting method is important for reproducing the *ab initio* data and calculating accurate collision integrals. Therefore, the NN PECs are used in the following calculations of collision integrals for the N–N and O–O interactions.

3.2.1. The collision integrals for N–N and O–O interactions. The collision integrals calculated with the present NN PECs for the N(^4S)–N(^4S,^2D,^2P) interactions are shown in table 6. It can be seen that the differences between the present and available data in the literature (Ding *et al* [34] and Levin *et al* [7]) are below 1% at $T \geqslant 5000$ K for the N(^4S)–N(^4S) interaction and about 7% at $T \leqslant 2000$ K. For collisions involving excited N atoms, namely N(^4S)–N(^2D) and N(^4S)–N(^2P), the present results of $\sigma^2\Omega^{(2,2)*}$ and elastic contribution of $\sigma^2\Omega^{(1,1)*}$ are in good agreement with those reported by Ding *et al* [34] (note that Levin *et al* [7] only reported the results of N(^4S)-N(^4S) interaction) except for very low temperatures. At low temperatures, the collision energy of particles is close to the PEC's fitting error, so the medium and long-range fitting accuracy would significantly influence the collision cross section. In addition to the elastic contribution, the inelastic contribution to diffusion collision integrals from the resonant excitation processes is also shown in table 6. To compute the inelastic contribution, we apply the NN function to fit the differences of the PECs for *gerade* and *ungerade* pairs. This is a more accurate way than the previous works [36, 37] which assumes the difference of PECs having an exponential functional form. It is obviously seen that the inelastic contribution to $\sigma^2\Omega^{(1,1)}$ is considerable and non-negligible, and its proportion increases as temperature increases (take up over 80% of the total values at high temperatures). Therefore, the present data of $\sigma^2\Omega^{(1,1)}$ are much greater than those of [34], which did not take the excitation exchange process (important for the excited atomic collisions) into account.

Similar comparisons are made for the O(^3P)–O(^3P), O(^3P)–O(^1D), and O(^1D)–O(^1D) interactions, and the results of collision integrals are shown in table 6. For the O(^3P)–O(^3P) interaction, it is observed that the differences between the present results and those of Levin *et al* [7] are below 4% except for $T \geqslant 500$ K. The difference between the data of Laricchiuta *et al* [37] and the present work is over 10%–27% for in the temperature range of 2000 K to 20 000 K. Differences between the present results and the data of Laricchiuta *et al* [37] are also found for the O(^3P)–O(^1D) and O(^1D)–O(^1D) interactions, which are about 16%–53% for viscous collision integrals in the same temperature. The discrepancies arise because of the lower accuracy of the PECs (see figure 9) used in [37]. Besides, the inelastic contribution (coming from the resonant excitation processes) to $\sigma^2\Omega^{(1,1)}$ is again remarkable for the O–O interactions, as seen from the results of the O(^3P)–O(^1D) collision in table 6.

In summary, all collision integrals results are tabulated in appendix, which includes the N(^4S, ^2D, ^2P)–N(^4S) and O(^3P, ^1D, ^1S)–O(^3P, ^1D, ^1S) interactions (with considering the inelastic contribution of $\sigma^2\Omega^{(1,1)}$) for a broad temperature range of 500–50 000 K.

Table 4. Comparison of the diffusion collision integrals $\sigma^2\Omega^{(1,1)*}$ (in Å^2) , denoted as (1,1), for the O(^3P)–O(^3P) and O(^3P)–O(^1D) interactions between the present results and the ones of Laricchiuta *et al* [37].

	O(^3P)–O(^3P)		O(^3P)–O(^1D)	
T(K)	$(1,1)^a$	$(1,1)^b$	$(1,1)^a$	$(1,1)^b$
2000	6.014	6.046	11.967	11.980
6000	4.257	4.248	9.982	9.980
10 000	3.525	3.516	9.217	9.218
18 000	2.770	2.788	8.452	8.472
20 000	2.645	2.652	8.327	8.332

[a] Laricchiuta *et al* [37]
[b] Present work.

Table 5. The viscous collision integrals $\sigma^2\Omega^{(2,2)*}$ (in Å^2) for the $X^1\Sigma_g^+$ $A'^5\Sigma_g^+$, and $2^3\Sigma_u^+$ states of the N–N system and the $X^3\Sigma_g^-$, $C^3\Delta_u$, and $^1\Pi_u$ states of the O–O system.

N–N									
	$X^1\Sigma_g^+$			$A'^5\Sigma_g^+$			$2^3\Sigma_u^+$		
T(K)	HH	MS	NN	HH	MS	NN	HH	MS	NN
500	11.75	7.71	8.29	7.16	5.76	5.09	8.50	12.62	7.30
2000	8.45	6.18	6.49	5.09	4.48	3.57	5.97	7.06	5.31
5000	6.55	5.21	5.28	3.34	3.18	3.01	4.76	5.02	4.22
10 000	5.34	4.52	4.47	2.36	2.32	2.35	3.49	3.70	3.38
20 000	4.37	3.91	3.89	1.83	1.82	1.84	2.10	2.27	2.34
40 000	3.22	3.05	3.08	1.51	1.51	1.51	1.26	1.34	1.48
O–O									
	$X^3\Sigma_g^-$			$^1\Pi_u$			$C^3\Delta_u$		
T(K)	HH	MS	NN	HH	MS	NN	HH	MS	NN
500	11.22	7.57	7.23	5.80	8.05	8.16	7.53	5.91	6.34
2000	8.06	6.00	5.27	4.62	5.36	5.67	5.42	4.70	4.54
5000	6.27	5.01	4.41	3.84	4.07	4.33	4.03	3.75	3.62
10 000	5.18	4.34	3.97	3.24	3.29	3.36	2.77	2.70	2.68
20 000	3.93	3.54	3.43	2.58	2.57	2.55	1.93	1.91	1.91
40 000	2.42	2.33	2.34	1.82	1.81	1.79	1.47	1.46	1.46

3.2.2. The collision model parameters for particle simulation. In many applications involving nonequilibrium weakly ionized plasma flows, the particle simulation methods, such as the direct simulation Monte Carlo (DSMC) and particle-in-cell with Monte Carlo collision (PIC-MCC), have to be adopted. In particle simulations, a specific collision model (collision cross section and scattering law), instead of the collision integral, is employed. However, reliable collision models for N–N and O–O interactions involving electronically excited states at high temperatures are lacking. For example, recent PIC-MCC simulation studies of capacitively coupled oxygen discharges assumed scattering of O atoms by O atoms to be half of the cross section for scattering of O atoms by O_2 molecules because of lacking reliable data [14, 80]. In a most recent work of developing collision models suitable for DSMC simulations of weakly ionized air, the contribution of excited state atoms was not taken into account [81].

In DSMC or PIC-MCC, the variable hard sphere (VHS) and variable soft sphere (VSS) models are the most widely used models for collisions between neutral particles. The total cross section (σ_T) and scattering angle (χ) for VHS and VSS models are given as,

$$\sigma_T(g) = C\pi d_{\text{ref}}^2 g^{-2\nu}, \tag{15}$$

$$\chi = 2\cos^{-1}\left(R_f^{1/\alpha}\right), \tag{16}$$

where C is a constant, g is the relative speed of the collision pair, and R_f is the ratio of the impact parameter to the sum of the radii of two colliding particles, which is a number randomly distributed in the range [0,1] in VHS and VSS models. d_{ref}, ν and α in equations (15) and (16) are the collision parameters to be determined. It is worth noting that the VSS model is reduced to the VHS model by letting $\alpha = 1$. For more details about VHS and VSS models, one can refer to Chapter 6 in [82].

With the collision integrals calculated in the last section, we can re-parameterize VHS and VSS models for N–N and O–O collision pairs with the contribution of excited state atoms

Table 6. The collision integrals (in Å^2) for the N–N and O–O interactions, where (1,1) and (2,2) represent the diffusion collision integrals $\sigma^2\Omega^{(1,1)*}$ and the viscous collision integrals $\sigma^2\Omega^{(2,2)*}$, respectively. Subscript *ex* is the inelastic contributions, and subscript *el* is the elastic contributions.

	N(^4S)–N(^4S)			N(^4S)–N(^2D)					
T(K)	$(2,2)^a$	$(2,2)^b$	$(2,2)^c$	$(2,2)^b$	$(2,2)^c$	$(1,1)^b$	$(1,1)_{el}{}^c$	$(1,1)_{ex}{}^c$	$(1,1)^c$
500	7.94	8.27	7.44	9.68	8.02	8.77	6.90	9.79	11.98
2000	5.82	5.83	5.66	6.68	6.22	5.89	5.35	9.46	10.87
5000	4.70	4.67	4.65	5.11	4.94	4.38	4.24	9.26	10.19
10 000	3.88	3.88	3.88	4.06	4.00	3.39	3.37	9.01	9.62
20 000	3.11	3.13	3.13	3.06	3.09	2.48	2.52	8.66	9.02
40 000	2.39	2.39	2.40	2.13	2.21	1.70	1.76	8.26	8.45
50 000	2.18	2.17	2.18	1.87	1.96	1.50	1.55	8.13	8.28
	N(^4S)–N(^4S)			N(^4S)–N(^2P)					
T(K)	$(1,1)^a$	$(1,1)^b$	$(1,1)^c$	$(2,2)^b$	$(2,2)^c$	$(1,1)^b$	$(1,1)_{el}{}^c$	$(1,1)_{ex}{}^c$	$(1,1)^c$
500	7.03	7.82	6.42	9.55	7.70	8.68	6.73	9.63	11.75
2000	5.15	5.23	4.91	6.45	5.84	5.72	5.09	9.12	10.49
5000	4.14	4.14	4.07	4.98	4.70	4.34	4.03	8.82	9.70
10 000	3.37	3.37	3.36	4.06	3.90	3.42	3.25	8.48	9.08
20 000	2.62	2.63	2.63	3.17	3.02	2.54	2.42	8.15	8.51
40 000	1.96	1.94	1.95	2.21	2.11	1.73	1.67	7.85	8.03
50 000	1.77	1.74	1.74	1.93	1.86	1.52	1.47	7.75	7.88
	O(^3P)–O(^3P)			O(^3P)–O(^1D)					
T(K)	$(2,2)^a$	$(2,2)^d$	$(2,2)^c$	$(2,2)^d$	$(2,2)^c$	$(1,1)^d$	$(1,1)_{el}{}^c$	$(1,1)_{ex}{}^c$	$(1,1)^c$
500	8.22		7.36		7.49		6.46	10.16	12.04
2000	5.58	6.97	5.46	8.58	5.41	11.97	4.65	9.18	10.29
4000	4.67	5.74	4.61	6.90	4.59	10.66	3.90	8.70	9.54
8000	3.88	4.59	3.84	5.40	3.86	9.54	3.23	8.23	8.85
20 000	2.91	3.24	2.94	3.71	3.00	8.33	2.46	7.67	8.05
40 000	2.26		2.33		2.43		1.95	7.26	7.51
50 000	2.07		2.14		2.25		1.79	7.12	7.34
	O(^3P)–O(^3P)			O(^1D)–O(^1D)					
T(K)	$(1,1)^a$	$(1,1)^d$	$(1,1)^c$	$(2,2)^d$	$(2,2)^c$	$(1,1)^d$	$(1,1)^c$		
500	7.28		6.41		7.04		6.16		
2000	4.84	6.01	4.68	8.21	5.35	7.02	4.63		
4000	4.00	4.88	3.94	6.53	4.52	5.43	3.85		
8000	3.27	3.84	3.25	5.00	3.73	4.05	3.13		
20 000	2.39	2.65	2.42	3.32	2.85	2.60	2.34		
40 000	1.81		1.87		2.29		1.84		
50 000	1.64		1.71		2.12		1.69		

[a] Levin *et al* [7].
[b] Ding *et al* [34].
[c] Present work.
[d] Laricchiuta *et al* [37].

included. For the VSS model, the viscous and diffusion collision integrals can be expressed as

$$\sigma^2\Omega^{(2,2)*} = \frac{\alpha d_{\text{ref}}^2}{(\alpha+1)(\alpha+2)}\left(\frac{T_{\text{ref}}}{T}\right)^{\nu}\frac{\Gamma(4-\nu)}{\Gamma(2-\nu)}, \tag{17}$$

$$\sigma^2\Omega^{(1,1)*} = \frac{d_{\text{ref}}^2}{(\alpha+1)}\left(\frac{T_{\text{ref}}}{T}\right)^{\nu}\frac{\Gamma(3-\nu)}{\Gamma(2-\nu)}, \tag{18}$$

where Γ is the gamma function, and T_{ref} is the reference temperature usually set to be 273 K. The collision model parameters d_{ref}, α, and ν are obtained by matching equations (15) and (16) against the corresponding collision integrals obtained in the last section. We find that a single set of model parameters can not fit the collision integral data well in the entire temperature range. Therefore, the temperature range is divided into three parts, i.e. 500–10 000 K, 10 000–20 000 K, and 20 000–50 000 K. The new model parameters are reported in table 7.

Table 7. Collision model parameters of VHS and VSS models for the N–N and O–O systems (T$\times 10^4$ K).

	VHS					VSS					
Collision type	d_{ref}(Å^2)	ν	α	Err.[a]	Err.[b]	d_{ref}(Å^2)	ν	α	Err.[a]	Err.[b]	T
N(^4S)–N(^4S)	3.205	0.211	1.000	3%	30%	3.157	0.211	1.403	3%	3%	0.05−1
	3.936	0.308	1.000	1%	30%	3.883	0.308	1.535	1%	2%	1−2
	4.894	0.390	1.000	1%	45%	4.850	0.390	1.749	1%	4%	2−5
N(^4S)–N(^2D)	3.330	0.240	1.000	6%	52%	3.830	0.229	0.503	6%	21%	0.05−1
	4.628	0.371	1.000	1%	60%	5.702	0.371	0.347	1%	9%	1−2
	6.398	0.493	1.000	1%	71%	8.635	0.493	0.261	1%	17%	2−5
N(^4S)–N(^2P)	3.328	0.227	1.000	3%	52%	3.739	0.227	0.490	3%	19%	0.05−1
	4.492	0.364	1.000	1%	59%	5.520	0.364	0.351	1%	9%	1−2
	6.980	0.529	1.000	1%	71%	9.302	0.529	0.271	1%	19%	2−5
O(^3P)–O(^3P)	3.29	0.236	1.000	2%	32%	3.219	0.238	1.457	2%	4%	0.05−1
	3.691	0.295	1.000	1%	35%	3.645	0.295	1.597	1%	2%	1−2
	4.206	0.345	1.000	1%	42%	4.167	0.345	1.735	1%	2%	2−5
O(^3P)–O(^1D)	3.277	0.239	1.000	2%	54%	3.735	0.239	0.461	2%	18%	0.05−1
	3.539	0.275	1.000	1%	59%	4.390	0.275	0.339	1%	6%	1−2
	3.920	0.314	1.000	1%	65%	5.112	0.314	0.289	1%	9%	2−5
O(^1D)–O(^1D)	3.200	0.232	1.000	4%	34%	3.154	0.232	1.442	4%	7%	0.05−1
	3.639	0.296	1.000	1%	35%	3.594	0.296	1.610	1%	1%	1−2
	3.870	0.319	1.000	1%	40%	3.831	0.319	1.707	1%	2%	2−5
O(^3P)–O(^1S)	2.891	0.183	1.000	1%	52%	3.320	0.183	0.448	1%	12%	0.05−1
	3.126	0.218	1.000	1%	55%	3.786	0.218	0.368	1%	4%	1−2
	3.937	0.306	1.000	1%	61%	4.927	0.306	0.330	1%	8%	2−5
O(^1D)–O(^1S)	3.330	0.240	1.000	2%	68%	3.848	0.240	0.437	2%	22%	0.05−1
	3.608	0.279	1.000	1%	63%	4.652	0.279	0.300	1%	6%	1−2
	3.779	0.296	1.000	1%	68%	5.124	0.296	0.257	1%	8%	2−5
O(^1S)–O(^1S)	2.697	0.147	1.000	1%	23%	2.660	0.147	1.308	1%	4%	0.05−1
	2.924	0.185	1.000	1%	28%	2.882	0.185	1.431	1%	1%	1−2
	3.346	0.236	1.000	1%	33%	3.301	0.236	1.548	1%	2%	2−5

[a] the fitting errors for viscous collision integrals.
[b] the fitting errors for diffusion collision integrals.

It can be seen that the fitting errors of viscous collision integrals are below 5% for both VHS and VSS models. The fitting errors of diffusion collision integrals are below 22% for the VSS model, while those for the VHS model are more than 50%.

4. Conclusions

The present work reports a complete set of high-accuracy collision integral data for N(^4S)–N(^4S, ^2D, ^2P) and O(^3P, ^1D, ^1S)–O(^3P, ^1D, ^1S) interactions in the temperature range of 500–50 000 K. Recent studies have highlighted the pivotal role of the quality of PECs in the accuracy of collision integral calculations in such a wide temperature range. The construction of high-quality PECs relies on both accurate potential energy data and function fitting method. In the present work, the potential energy data are computed by using the icMRCI method with the Davidson correction and basis-set extrapolation. The extrapolation adopts the aug-cc-pVQZ and aug-cc-pV5Z basis sets. Special attentions have been paid to include more Rydberg configurations and to expand the calculation to short-range regions to ensure the accuracy of collision integrals at high temperatures. In light of the existence of avoided crossings, the diabatic representation of the PECs is chosen in the present work because its fitting accuracy and robustness in collision integral calculations outperform the adiabatic representation. More importantly, based on the Zhu-Nakamura theory [77, 78], the present study showed that the diabatic paths in collisions are much more likely to be followed than the adiabatic paths through the avoided crossings. The potential energy data calculated by the high-level *ab initio* method are compared with the available experimental data and an excellent agreement is achieved. The HH, MS, and NN models are used to fit the potential energy data. Though considered to be the best general purpose atom-atom potentials, the HH and MS models are found to be incapable of accurately fitting the data in a wide energy range for all the electronic states, especially when multiple extrema exist in the PECs. Instead, the NN can achieve very high fitting accuracy for all interactions considered in the present work.

The newly developed high-quality NN PECs are then applied to calculate the collision integrals. When the atoms in different electronically excited states are involved, it is important to consider the contribution of inelastic resonant excitation exchange interactions to the diffusion collision integrals, which can take up over 80% of the total values at

high temperatures. To compute the excitation exchange collision integrals, one needs the differences of PECs for *gerade* and *ungerade* pairs. Almost all previous works assumed the difference of PECs to have an exponential functional form. However, it is found that the exponential function is crude to represent all relevant interactions. In order to achieve high accuracy also in the calculation of excitation exchange collision integrals, we again apply the NN function to fit the differences of the PECs for *gerade* and *ungerade* pairs.

By taking all measures mentioned above to ensure high accuracy, the collision integral calculations in this work are believed to be highly reliable. The reported data supplement the database of high-accuracy collision integrals as well as the transport properties of atomic species in both ground and electronically excited states in weakly ionized air plasmas. Work is in progress for other important interactions in air plasmas, such as the collisions between atomic N and O as well as those involving charged species.

Data availability statement

All data that support the findings of this study are included within the article (and any supplementary files).

Acknowledgment

Q Hong acknowledges the fellowship of China Postdoctoral Science Foundation (Grant No. 2022M723233) and the National Natural Science Foundation of China (Grant No. 12302391). The authors would like to thank Dr Zhi Qin and Dr Ryan Brady for the helpful discussions.

Appendix. Collision integrals

Table A1. The collision integrals ($Å^2$) for N(^{4}S)–N(^{4}S) interaction.

T(K)	$\sigma^2\Omega^{(1,1)*}$	$\sigma^2\Omega^{(1,2)*}$	$\sigma^2\Omega^{(1,3)*}$	$\sigma^2\Omega^{(1,4)*}$	$\sigma^2\Omega^{(2,2)*}$	$\sigma^2\Omega^{(2,3)*}$	$\sigma^2\Omega^{(2,4)*}$	$\sigma^2\Omega^{(3,3)*}$
500	6.42	6.00	5.69	5.46	7.44	7.05	6.76	6.62
800	5.84	5.46	5.19	5.00	6.76	6.42	6.17	6.03
1000	5.59	5.23	4.99	4.81	6.47	6.15	5.91	5.78
1200	5.40	5.06	4.83	4.66	6.24	5.93	5.71	5.59
1400	5.24	4.92	4.70	4.53	6.06	5.76	5.55	5.44
1600	5.12	4.80	4.59	4.42	5.90	5.62	5.41	5.31
1800	5.01	4.70	4.48	4.31	5.77	5.50	5.29	5.19
2000	4.91	4.61	4.39	4.21	5.66	5.39	5.18	5.09
2500	4.71	4.41	4.18	3.99	5.42	5.15	4.94	4.87
3000	4.55	4.24	4.01	3.81	5.23	4.95	4.73	4.68
3500	4.40	4.09	3.85	3.65	5.06	4.78	4.55	4.51
4000	4.28	3.96	3.71	3.51	4.90	4.62	4.39	4.37
4500	4.17	3.84	3.59	3.39	4.77	4.49	4.25	4.24
5000	4.07	3.74	3.48	3.28	4.65	4.37	4.13	4.12
5500	3.97	3.64	3.38	3.18	4.54	4.26	4.03	4.01
6000	3.88	3.55	3.29	3.08	4.44	4.16	3.93	3.91
7000	3.73	3.39	3.13	2.92	4.27	3.99	3.77	3.73
8000	3.59	3.25	2.99	2.77	4.12	3.84	3.63	3.58
9000	3.47	3.13	2.86	2.65	3.99	3.72	3.50	3.45
10 000	3.36	3.01	2.75	2.53	3.88	3.60	3.39	3.33
12 000	3.17	2.82	2.55	2.34	3.68	3.41	3.19	3.13
14 000	3.01	2.66	2.39	2.19	3.51	3.24	3.03	2.96
16 000	2.87	2.52	2.26	2.05	3.37	3.10	2.88	2.81
18 000	2.74	2.39	2.14	1.94	3.24	2.97	2.76	2.69
20 000	2.63	2.29	2.03	1.84	3.13	2.86	2.65	2.58
25 000	2.40	2.07	1.82	1.64	2.89	2.63	2.42	2.35
30 000	2.22	1.89	1.66	1.49	2.70	2.44	2.24	2.17
35 000	2.07	1.75	1.53	1.36	2.54	2.28	2.08	2.02
40 000	1.95	1.64	1.42	1.26	2.40	2.15	1.95	1.90
45 000	1.84	1.54	1.33	1.18	2.29	2.04	1.84	1.80
50 000	1.74	1.45	1.25	1.11	2.18	1.93	1.74	1.71

Table A2. The collision integrals (Å^2) for N(^{4}S)–N(^{2}D) interaction.

T(K)	$\sigma^2\Omega_{el}^{(1,1)*}$	$\sigma^2\Omega^{(1,1)*}$	$\sigma^2\Omega^{(1,2)*}$	$\sigma^2\Omega^{(1,3)*}$	$\sigma^2\Omega^{(1,4)*}$	$\sigma^2\Omega^{(2,2)*}$	$\sigma^2\Omega^{(2,3)*}$	$\sigma^2\Omega^{(2,4)*}$	$\sigma^2\Omega^{(3,3)*}$
500	6.90	11.98	6.57	6.32	6.11	8.02	7.75	7.52	7.23
800	6.42	11.57	6.06	5.77	5.53	7.48	7.17	6.90	6.69
1000	6.18	11.39	5.80	5.50	5.25	7.19	6.86	6.58	6.40
1200	5.97	11.25	5.58	5.27	5.02	6.95	6.60	6.31	6.17
1400	5.78	11.13	5.39	5.08	4.83	6.73	6.37	6.08	5.97
1600	5.62	11.03	5.22	4.92	4.67	6.54	6.18	5.89	5.79
1800	5.48	10.94	5.08	4.77	4.53	6.37	6.01	5.72	5.63
2000	5.35	10.87	4.95	4.65	4.40	6.22	5.86	5.57	5.49
2500	5.09	10.71	4.68	4.37	4.13	5.90	5.54	5.27	5.19
3000	4.87	10.58	4.46	4.15	3.90	5.64	5.29	5.02	4.94
3500	4.67	10.46	4.27	3.96	3.70	5.43	5.09	4.81	4.73
4000	4.51	10.36	4.10	3.79	3.54	5.25	4.90	4.63	4.55
4500	4.37	10.27	3.95	3.64	3.39	5.09	4.74	4.47	4.40
5000	4.23	10.19	3.82	3.51	3.25	4.94	4.60	4.33	4.25
5500	4.12	10.11	3.70	3.39	3.14	4.81	4.47	4.20	4.12
6000	4.01	10.04	3.59	3.28	3.03	4.69	4.35	4.08	4.01
7000	3.82	9.92	3.40	3.09	2.84	4.48	4.14	3.87	3.80
8000	3.65	9.81	3.23	2.92	2.67	4.30	3.96	3.70	3.62
9000	3.50	9.71	3.08	2.77	2.53	4.14	3.81	3.54	3.46
10 000	3.37	9.62	2.95	2.64	2.40	4.00	3.67	3.41	3.32
12 000	3.14	9.47	2.73	2.42	2.18	3.76	3.43	3.17	3.09
14 000	2.95	9.33	2.54	2.24	2.00	3.56	3.23	2.97	2.89
16 000	2.79	9.22	2.38	2.08	1.86	3.38	3.05	2.79	2.72
18 000	2.64	9.11	2.24	1.95	1.73	3.23	2.90	2.64	2.58
20 000	2.52	9.02	2.12	1.84	1.63	3.09	2.76	2.50	2.45
25 000	2.26	8.83	1.88	1.62	1.43	2.80	2.47	2.22	2.19
30 000	2.05	8.68	1.69	1.45	1.28	2.57	2.25	2.01	1.99
35 000	1.89	8.55	1.55	1.32	1.16	2.37	2.07	1.84	1.84
40 000	1.76	8.45	1.43	1.22	1.07	2.21	1.92	1.70	1.71
45 000	1.64	8.36	1.34	1.14	1.00	2.08	1.79	1.59	1.60
50 000	1.55	8.28	1.25	1.07	0.94	1.96	1.69	1.49	1.51

Table A3. The collision integrals (Å^2) for N(^{4}S)–N(^{2}P) interaction.

T(K)	$\sigma^2\Omega_{el}^{(1,1)*}$	$\sigma^2\Omega^{(1,1)*}$	$\sigma^2\Omega^{(1,2)*}$	$\sigma^2\Omega^{(1,3)*}$	$\sigma^2\Omega^{(1,4)*}$	$\sigma^2\Omega^{(2,2)*}$	$\sigma^2\Omega^{(2,3)*}$	$\sigma^2\Omega^{(2,4)*}$	$\sigma^2\Omega^{(3,3)*}$
500	6.73	11.75	6.39	6.11	5.86	7.70	7.42	7.17	6.95
800	6.21	11.31	5.82	5.50	5.24	7.12	6.78	6.49	6.34
1000	5.94	11.10	5.53	5.21	4.96	6.81	6.46	6.17	6.03
1200	5.71	10.93	5.30	4.99	4.74	6.55	6.19	5.91	5.79
1400	5.52	10.79	5.11	4.80	4.57	6.33	5.98	5.70	5.58
1600	5.36	10.68	4.95	4.65	4.42	6.14	5.80	5.53	5.41
1800	5.21	10.57	4.81	4.51	4.29	5.98	5.64	5.38	5.26
2000	5.09	10.49	4.68	4.39	4.17	5.84	5.50	5.25	5.13
2500	4.82	10.30	4.43	4.15	3.93	5.54	5.22	4.98	4.86
3000	4.61	10.14	4.22	3.95	3.73	5.32	5.00	4.77	4.64
3500	4.43	10.01	4.05	3.78	3.56	5.13	4.82	4.59	4.46
4000	4.28	9.90	3.91	3.63	3.41	4.97	4.67	4.44	4.31
4500	4.15	9.79	3.78	3.50	3.28	4.83	4.53	4.30	4.17
5000	4.03	9.70	3.66	3.38	3.16	4.70	4.41	4.18	4.05
5500	3.92	9.62	3.55	3.27	3.04	4.59	4.30	4.07	3.94
6000	3.83	9.54	3.45	3.17	2.94	4.49	4.20	3.97	3.84
7000	3.65	9.40	3.28	2.99	2.76	4.31	4.02	3.79	3.65
8000	3.50	9.28	3.13	2.83	2.59	4.16	3.87	3.63	3.49
9000	3.37	9.18	2.99	2.69	2.45	4.02	3.73	3.49	3.35
10 000	3.25	9.08	2.86	2.56	2.31	3.90	3.60	3.36	3.22
12 000	3.03	8.93	2.64	2.34	2.09	3.68	3.37	3.12	2.99
14 000	2.85	8.80	2.45	2.15	1.91	3.49	3.17	2.91	2.80
16 000	2.69	8.68	2.29	1.99	1.76	3.32	2.99	2.72	2.64
18 000	2.55	8.59	2.15	1.86	1.63	3.16	2.83	2.56	2.49
20 000	2.42	8.51	2.03	1.74	1.53	3.02	2.69	2.41	2.37
25 000	2.16	8.34	1.78	1.52	1.34	2.72	2.38	2.11	2.11
30 000	1.96	8.21	1.60	1.36	1.20	2.48	2.15	1.89	1.91
35 000	1.80	8.11	1.46	1.24	1.10	2.28	1.96	1.73	1.75
40 000	1.67	8.03	1.35	1.15	1.02	2.11	1.81	1.59	1.62
45 000	1.56	7.97	1.26	1.08	0.96	1.97	1.69	1.49	1.52
50 000	1.47	7.88	1.19	1.02	0.91	1.86	1.59	1.40	1.43

Table A4. The collision integrals ($Å^2$) for $O(^3P)$–$O(^3P)$ interaction.

T(K)	$\sigma^2\Omega^{(1,1)*}$	$\sigma^2\Omega^{(1,2)*}$	$\sigma^2\Omega^{(1,3)*}$	$\sigma^2\Omega^{(1,4)*}$	$\sigma^2\Omega^{(2,2)*}$	$\sigma^2\Omega^{(2,3)*}$	$\sigma^2\Omega^{(2,4)*}$	$\sigma^2\Omega^{(3,3)*}$
500	6.41	5.96	5.63	5.38	7.36	7.03	6.76	6.52
800	5.78	5.35	5.04	4.80	6.71	6.36	6.08	5.89
1000	5.50	5.09	4.78	4.56	6.41	6.05	5.77	5.61
1200	5.28	4.87	4.58	4.36	6.14	5.79	5.52	5.38
1400	5.10	4.70	4.42	4.20	5.94	5.59	5.32	5.19
1600	4.93	4.54	4.27	4.06	5.74	5.41	5.15	5.03
1800	4.80	4.42	4.15	3.94	5.59	5.26	5.01	4.89
2000	4.68	4.31	4.04	3.83	5.46	5.13	4.88	4.77
2500	4.44	4.07	3.81	3.61	5.17	4.86	4.62	4.51
3000	4.24	3.88	3.63	3.43	4.95	4.65	4.42	4.30
3500	4.08	3.73	3.48	3.28	4.77	4.47	4.25	4.13
4000	3.94	3.59	3.35	3.15	4.61	4.32	4.10	3.99
4500	3.82	3.48	3.23	3.04	4.48	4.19	3.97	3.87
5000	3.71	3.37	3.13	2.94	4.36	4.08	3.86	3.75
5500	3.61	3.28	3.04	2.86	4.25	3.97	3.76	3.66
6000	3.53	3.20	2.96	2.78	4.16	3.88	3.66	3.57
7000	3.38	3.05	2.82	2.64	3.99	3.72	3.51	3.41
8000	3.25	2.93	2.70	2.53	3.84	3.58	3.37	3.28
9000	3.14	2.82	2.60	2.42	3.72	3.46	3.26	3.16
10 000	3.04	2.73	2.51	2.34	3.61	3.36	3.16	3.06
12 000	2.87	2.57	2.35	2.18	3.43	3.18	2.99	2.89
14 000	2.73	2.44	2.22	2.06	3.28	3.04	2.85	2.75
16 000	2.62	2.32	2.12	1.95	3.15	2.91	2.73	2.63
18 000	2.51	2.23	2.02	1.86	3.04	2.80	2.62	2.53
20 000	2.42	2.14	1.94	1.79	2.94	2.71	2.53	2.43
25 000	2.24	1.97	1.77	1.63	2.74	2.51	2.34	2.25
30 000	2.09	1.83	1.64	1.50	2.57	2.36	2.19	2.10
35 000	1.97	1.71	1.54	1.40	2.44	2.23	2.06	1.98
40 000	1.87	1.62	1.45	1.32	2.33	2.12	1.95	1.88
45 000	1.78	1.54	1.37	1.25	2.23	2.02	1.86	1.80
50 000	1.71	1.47	1.31	1.19	2.14	1.94	1.78	1.72

Table A5. The collision integrals (Å^2) for O(^{3}P)–O(^{1}D) interaction.

T(K)	$\sigma^2\Omega_{el}^{(1,1)*}$	$\sigma^2\Omega^{(1,1)*}$	$\sigma^2\Omega^{(1,2)*}$	$\sigma^2\Omega^{(1,3)*}$	$\sigma^2\Omega^{(1,4)*}$	$\sigma^2\Omega^{(2,2)*}$	$\sigma^2\Omega^{(2,3)*}$	$\sigma^2\Omega^{(2,4)*}$	$\sigma^2\Omega^{(3,3)*}$
500	6.46	12.04	6.00	5.63	5.37	7.49	7.09	6.78	6.58
800	5.80	11.40	5.36	5.00	4.77	6.75	6.30	6.00	5.86
1000	5.50	11.12	5.07	4.75	4.52	6.38	5.98	5.70	5.56
1200	5.28	10.90	4.83	4.55	4.33	6.09	5.73	5.46	5.32
1400	5.06	10.70	4.66	4.38	4.17	5.88	5.53	5.27	5.13
1600	4.89	10.54	4.51	4.24	4.03	5.69	5.36	5.11	4.96
1800	4.77	10.41	4.38	4.12	3.91	5.54	5.22	4.98	4.82
2000	4.65	10.29	4.27	4.01	3.80	5.41	5.09	4.85	4.70
2500	4.40	10.04	4.04	3.78	3.57	5.13	4.83	4.60	4.45
3000	4.21	9.85	3.85	3.60	3.40	4.92	4.63	4.40	4.25
3500	4.05	9.68	3.70	3.45	3.26	4.74	4.46	4.24	4.09
4000	3.90	9.54	3.56	3.32	3.13	4.59	4.32	4.10	3.95
4500	3.79	9.42	3.45	3.21	3.03	4.46	4.19	3.98	3.83
5000	3.68	9.31	3.35	3.12	2.94	4.35	4.08	3.87	3.72
5500	3.59	9.21	3.26	3.03	2.86	4.24	3.98	3.77	3.63
6000	3.50	9.12	3.18	2.96	2.78	4.15	3.89	3.69	3.55
7000	3.36	8.97	3.05	2.83	2.66	3.99	3.74	3.54	3.40
8000	3.23	8.85	2.93	2.72	2.55	3.86	3.61	3.42	3.28
9000	3.13	8.74	2.83	2.62	2.46	3.74	3.50	3.31	3.17
10 000	3.03	8.64	2.74	2.54	2.38	3.64	3.40	3.21	3.08
12 000	2.88	8.48	2.59	2.39	2.24	3.47	3.23	3.05	2.92
14 000	2.75	8.35	2.47	2.28	2.13	3.32	3.09	2.92	2.80
16 000	2.64	8.24	2.37	2.18	2.03	3.20	2.98	2.81	2.69
18 000	2.55	8.14	2.28	2.09	1.95	3.10	2.88	2.71	2.59
20 000	2.46	8.05	2.20	2.02	1.87	3.01	2.79	2.62	2.51
25 000	2.29	7.87	2.04	1.86	1.72	2.82	2.61	2.44	2.33
30 000	2.15	7.73	1.91	1.73	1.60	2.66	2.46	2.30	2.20
35 000	2.04	7.61	1.80	1.63	1.50	2.54	2.33	2.18	2.08
40 000	1.95	7.51	1.71	1.54	1.42	2.43	2.23	2.07	1.99
45 000	1.86	7.42	1.63	1.47	1.34	2.34	2.14	1.98	1.90
50 000	1.79	7.34	1.57	1.40	1.28	2.25	2.05	1.90	1.83

Table A6. The collision integrals (Å^2) for O(^{1}D)–O(^{1}D) interaction.

T(K)	$\sigma^2\Omega^{(1,1)*}$	$\sigma^2\Omega^{(1,2)*}$	$\sigma^2\Omega^{(1,3)*}$	$\sigma^2\Omega^{(1,4)*}$	$\sigma^2\Omega^{(2,2)*}$	$\sigma^2\Omega^{(2,3)*}$	$\sigma^2\Omega^{(2,4)*}$	$\sigma^2\Omega^{(3,3)*}$
500	6.16	5.84	5.58	5.35	7.04	6.76	6.52	6.35
800	5.67	5.31	5.02	4.79	6.48	6.18	5.93	5.78
1000	5.44	5.06	4.76	4.52	6.21	5.90	5.65	5.51
1200	5.22	4.84	4.55	4.31	5.98	5.67	5.42	5.28
1400	5.04	4.66	4.37	4.14	5.79	5.48	5.23	5.09
1600	4.89	4.50	4.22	3.99	5.62	5.32	5.07	4.93
1800	4.76	4.37	4.08	3.86	5.48	5.17	4.93	4.79
2000	4.63	4.25	3.97	3.75	5.35	5.04	4.80	4.67
2500	4.38	4.00	3.72	3.50	5.08	4.78	4.54	4.40
3000	4.17	3.80	3.52	3.31	4.86	4.56	4.33	4.19
3500	4.00	3.63	3.36	3.16	4.68	4.38	4.15	4.02
4000	3.85	3.49	3.23	3.02	4.52	4.22	3.99	3.87
4500	3.73	3.37	3.11	2.91	4.38	4.09	3.86	3.74
5000	3.61	3.26	3.01	2.82	4.26	3.97	3.74	3.62
5500	3.51	3.16	2.92	2.73	4.15	3.86	3.64	3.52
6000	3.42	3.08	2.84	2.66	4.05	3.77	3.55	3.43
7000	3.27	2.93	2.70	2.53	3.88	3.60	3.39	3.28
8000	3.13	2.81	2.59	2.42	3.73	3.46	3.26	3.15
9000	3.02	2.71	2.49	2.33	3.61	3.34	3.15	3.04
10 000	2.92	2.62	2.41	2.25	3.50	3.24	3.05	2.94
12 000	2.76	2.47	2.27	2.12	3.31	3.07	2.89	2.78
14 000	2.63	2.35	2.15	2.01	3.17	2.93	2.76	2.65
16 000	2.52	2.25	2.06	1.92	3.04	2.82	2.65	2.54
18 000	2.42	2.16	1.98	1.84	2.94	2.72	2.55	2.45
20 000	2.34	2.08	1.90	1.77	2.85	2.63	2.47	2.37
25 000	2.17	1.93	1.76	1.62	2.66	2.46	2.30	2.20
30 000	2.04	1.80	1.64	1.51	2.51	2.32	2.16	2.07
35 000	1.93	1.70	1.54	1.41	2.39	2.20	2.05	1.96
40 000	1.84	1.62	1.46	1.34	2.29	2.10	1.95	1.87
45 000	1.76	1.54	1.39	1.27	2.20	2.01	1.86	1.79
50 000	1.69	1.48	1.33	1.21	2.12	1.93	1.79	1.72

Table A7. The collision integrals (Å^2) for O(^{3}P)–O(^{1}S) interaction.

T(K)	$\sigma^2\Omega_{el}^{(1,1)*}$	$\sigma^2\Omega^{(1,1)*}$	$\sigma^2\Omega^{(1,2)*}$	$\sigma^2\Omega^{(1,3)*}$	$\sigma^2\Omega^{(1,4)*}$	$\sigma^2\Omega^{(2,2)*}$	$\sigma^2\Omega^{(2,3)*}$	$\sigma^2\Omega^{(2,4)*}$	$\sigma^2\Omega^{(3,3)*}$
500	5.62	10.59	5.25	4.99	4.80	6.38	6.08	5.86	5.67
800	5.13	10.21	4.80	4.57	4.40	5.85	5.58	5.38	5.21
1000	4.91	10.06	4.60	4.38	4.22	5.62	5.36	5.17	5.00
1200	4.75	9.94	4.45	4.24	4.08	5.43	5.19	5.00	4.84
1400	4.61	9.84	4.32	4.12	3.96	5.28	5.04	4.86	4.70
1600	4.49	9.74	4.21	4.01	3.86	5.16	4.92	4.75	4.59
1800	4.40	9.65	4.12	3.92	3.77	5.05	4.82	4.65	4.49
2000	4.31	9.57	4.04	3.85	3.70	4.95	4.73	4.56	4.40
2500	4.13	9.39	3.87	3.68	3.53	4.76	4.55	4.38	4.22
3000	3.99	9.23	3.73	3.55	3.40	4.61	4.40	4.24	4.08
3500	3.87	9.09	3.62	3.43	3.29	4.48	4.28	4.12	3.96
4000	3.77	8.97	3.52	3.34	3.19	4.37	4.18	4.02	3.85
4500	3.68	8.86	3.43	3.25	3.11	4.28	4.09	3.93	3.76
5000	3.60	8.76	3.36	3.18	3.03	4.20	4.01	3.85	3.69
5500	3.53	8.68	3.29	3.11	2.96	4.12	3.93	3.78	3.61
6000	3.47	8.60	3.23	3.05	2.90	4.06	3.87	3.71	3.55
7000	3.36	8.47	3.11	2.93	2.79	3.94	3.75	3.60	3.43
8000	3.26	8.35	3.02	2.84	2.69	3.84	3.65	3.50	3.34
9000	3.18	8.25	2.93	2.75	2.61	3.75	3.56	3.41	3.25
10 000	3.10	8.17	2.86	2.68	2.53	3.67	3.48	3.34	3.17
12 000	2.97	8.02	2.72	2.54	2.39	3.54	3.35	3.20	3.03
14 000	2.85	7.89	2.61	2.42	2.27	3.42	3.24	3.09	2.92
16 000	2.76	7.78	2.51	2.32	2.16	3.32	3.14	2.98	2.81
18 000	2.67	7.69	2.42	2.23	2.07	3.23	3.04	2.89	2.72
20 000	2.59	7.56	2.34	2.14	1.98	3.15	2.96	2.80	2.64
25 000	2.42	7.43	2.16	1.97	1.81	2.98	2.77	2.60	2.47
30 000	2.28	7.28	2.02	1.82	1.67	2.83	2.61	2.44	2.32
35 000	2.16	7.16	1.90	1.71	1.57	2.69	2.48	2.30	2.20
40 000	2.06	7.06	1.80	1.62	1.48	2.58	2.36	2.17	2.10
45 000	1.97	6.97	1.71	1.54	1.40	2.47	2.25	2.07	2.01
50 000	1.89	6.89	1.64	1.47	1.34	2.38	2.15	1.98	1.93

Table A8. The collision integrals (Å^2) for O(^{1}D)–O(^{1}S) interaction.

T(K)	$\sigma^2\Omega_{el}^{(1,1)*}$	$\sigma^2\Omega^{(1,1)*}$	$\sigma^2\Omega^{(1,2)*}$	$\sigma^2\Omega^{(1,3)*}$	$\sigma^2\Omega^{(1,4)*}$	$\sigma^2\Omega^{(2,2)*}$	$\sigma^2\Omega^{(2,3)*}$	$\sigma^2\Omega^{(2,4)*}$	$\sigma^2\Omega^{(3,3)*}$
500	6.59	12.19	6.20	5.88	5.62	7.63	7.30	7.01	6.80
800	6.01	11.80	5.59	5.26	5.00	6.96	6.58	6.27	6.14
1000	5.73	11.63	5.29	4.97	4.72	6.62	6.24	5.93	5.82
1200	5.49	11.49	5.06	4.75	4.51	6.34	5.96	5.66	5.56
1400	5.29	11.37	4.87	4.57	4.34	6.11	5.74	5.45	5.36
1600	5.13	11.28	4.71	4.42	4.19	5.91	5.55	5.28	5.18
1800	4.98	11.19	4.58	4.29	4.07	5.74	5.39	5.13	5.03
2000	4.85	11.12	4.46	4.17	3.96	5.60	5.26	5.00	4.90
2500	4.59	10.96	4.21	3.93	3.72	5.30	4.98	4.74	4.62
3000	4.38	10.84	4.01	3.74	3.53	5.08	4.77	4.54	4.41
3500	4.21	10.73	3.84	3.58	3.37	4.89	4.59	4.37	4.23
4000	4.07	10.63	3.70	3.44	3.24	4.73	4.44	4.22	4.08
4500	3.94	10.54	3.58	3.32	3.12	4.60	4.31	4.09	3.96
5000	3.83	10.46	3.47	3.22	3.03	4.48	4.19	3.97	3.84
5500	3.73	10.38	3.38	3.13	2.94	4.37	4.09	3.87	3.74
6000	3.63	10.31	3.29	3.05	2.86	4.27	3.99	3.77	3.65
7000	3.48	10.18	3.14	2.91	2.73	4.10	3.83	3.61	3.50
8000	3.35	10.06	3.02	2.79	2.62	3.96	3.69	3.48	3.37
9000	3.23	9.96	2.92	2.70	2.53	3.83	3.57	3.37	3.26
10 000	3.13	9.86	2.82	2.61	2.45	3.72	3.46	3.27	3.16
12 000	2.97	9.68	2.67	2.47	2.32	3.54	3.29	3.11	2.99
14 000	2.83	9.53	2.55	2.35	2.21	3.39	3.15	2.98	2.86
16 000	2.72	9.40	2.45	2.26	2.11	3.26	3.04	2.87	2.75
18 000	2.63	9.29	2.36	2.17	2.03	3.16	2.94	2.77	2.66
20 000	2.54	9.18	2.28	2.10	1.96	3.07	2.85	2.69	2.58
25 000	2.37	8.96	2.12	1.95	1.81	2.88	2.67	2.52	2.41
30 000	2.24	8.79	2.00	1.83	1.69	2.73	2.53	2.38	2.27
35 000	2.13	8.64	1.89	1.73	1.60	2.61	2.41	2.26	2.17
40 000	2.03	8.52	1.80	1.64	1.52	2.51	2.31	2.16	2.07
45 000	1.95	8.23	1.73	1.57	1.45	2.42	2.22	2.07	1.99
50 000	1.88	8.13	1.66	1.51	1.40	2.33	2.14	1.99	1.92

Table A9. The collision integrals (Å^2) for O(^{1}S)–O(^{1}S) interaction.

T(K)	$\sigma^2\Omega^{(1,1)*}$	$\sigma^2\Omega^{(1,2)*}$	$\sigma^2\Omega^{(1,3)*}$	$\sigma^2\Omega^{(1,4)*}$	$\sigma^2\Omega^{(2,2)*}$	$\sigma^2\Omega^{(2,3)*}$	$\sigma^2\Omega^{(2,4)*}$	$\sigma^2\Omega^{(3,3)*}$
500	5.32	5.01	4.81	4.66	5.89	5.63	5.44	5.33
800	4.92	4.65	4.47	4.34	5.45	5.24	5.09	4.95
1000	4.75	4.50	4.32	4.19	5.27	5.08	4.94	4.78
1200	4.61	4.37	4.20	4.07	5.13	4.95	4.82	4.66
1400	4.50	4.27	4.10	3.97	5.02	4.85	4.72	4.56
1600	4.41	4.18	4.02	3.89	4.93	4.76	4.63	4.47
1800	4.33	4.10	3.94	3.81	4.85	4.68	4.55	4.39
2000	4.26	4.04	3.87	3.75	4.78	4.62	4.49	4.32
2500	4.11	3.89	3.73	3.61	4.63	4.47	4.34	4.18
3000	3.99	3.78	3.62	3.49	4.52	4.35	4.23	4.06
3500	3.89	3.68	3.52	3.39	4.42	4.26	4.13	3.96
4000	3.81	3.59	3.43	3.31	4.33	4.17	4.04	3.88
4500	3.73	3.52	3.36	3.23	4.25	4.09	3.97	3.80
5000	3.66	3.45	3.29	3.17	4.19	4.03	3.90	3.74
5500	3.60	3.39	3.23	3.11	4.13	3.97	3.84	3.68
6000	3.55	3.34	3.18	3.05	4.07	3.91	3.78	3.62
7000	3.45	3.24	3.08	2.95	3.97	3.81	3.68	3.52
8000	3.36	3.15	2.99	2.86	3.89	3.73	3.60	3.44
9000	3.29	3.08	2.92	2.79	3.81	3.65	3.52	3.36
10 000	3.22	3.01	2.85	2.72	3.74	3.58	3.45	3.29
12 000	3.11	2.89	2.73	2.60	3.63	3.47	3.34	3.17
14 000	3.01	2.79	2.63	2.49	3.53	3.36	3.23	3.07
16 000	2.92	2.70	2.54	2.41	3.44	3.28	3.14	2.98
18 000	2.84	2.63	2.46	2.33	3.36	3.20	3.06	2.91
20 000	2.77	2.56	2.39	2.26	3.29	3.13	2.99	2.84
25 000	2.63	2.41	2.24	2.11	3.14	2.97	2.83	2.69
30 000	2.51	2.29	2.12	1.99	3.02	2.84	2.70	2.57
35 000	2.40	2.18	2.02	1.89	2.91	2.73	2.58	2.46
40 000	2.32	2.10	1.93	1.81	2.81	2.63	2.48	2.37
45 000	2.24	2.02	1.86	1.74	2.73	2.54	2.39	2.30
50 000	2.17	1.95	1.80	1.68	2.65	2.46	2.31	2.23

ORCID iDs

Qizhen Hong https://orcid.org/0000-0003-3188-9167
Chao Yang https://orcid.org/0000-0002-5592-7538
Quanhua Sun https://orcid.org/0000-0002-0008-1790
Yuan Hu https://orcid.org/0000-0001-6870-183X

References

[1] Schouler M, Prevereaud Y and Mieussens L 2020 Survey of flight and numerical data of hypersonic rarefied flows encountered in earth orbit and atmospheric reentry *Prog. Aerosp. Sci.* **118** 100638
[2] Andreussi E, Ferrato T and Giannetti V 2022 A review of air-breathing electric propulsion: from mission studies to technology verification *J. Electr. Propuls.* **1** 1–57
[3] Liu S, Trelles J P, Li C, Li C and Guo H 2022 A review and progress of multiphase flows in atmospheric and low pressure plasma spray advanced coating *Mater. Today Phys.* **27** 100832
[4] Anders A 2017 Tutorial: reactive high power impulse magnetron sputtering (r-hipims) *J. Appl. Phys.* **121** 7
[5] Chapman S and Cowling T G 1952 *The Mathematical Theory of Non-Uniform Gases : An Account of the Kinetic Theory of Viscosity, Thermal Conduction and Diffusion in Gases* (Cambridge University Press)
[6] Hirschfelder J O, Curtiss C F and Bird R B 1954 *Molecular Theory of Gases and Liquids* (Wiley)
[7] Levin E, Partridge H and Stallcop J R 1990 Collision integrals and high temperature transport properties for N-N, O-O and N-O *J. Thermophys. Heat Transfer* **4** 469–77
[8] Capitelli M, Giordano D, Gorse C and Longo S 2000 Collision integrals of high-temperature air species *J. Thermophys. Heat Transfer* **14** 259–68
[9] Capitelli M, Bruno D and Laricchiuta A 2013 *Transport Cross Sections: Classical and Quantum Approaches* vol 74 (Springer) pp 57–98
[10] Buchowiecki M and Szabo P 2023 On the usefulness of the classical description of collision integrals of interacting atoms/ions. collision integrals for O(^{3}P)-O(^{3}P) interaction
[11] Wright M J, Bose D, Palmer G E and Levin E 2005 Recommended collision integrals for transport property computations part 1: air species *AIAA J.* **43** 2558–64
[12] Titova N S Starik A M and Arsentiev I V 2010 Comprehensive analysis of the effect of atomic and molecular metastable state excitation on air plasma composition behind strong shock waves *Plasma Sources Sci. Technol.* **19** 015007
[13] Kozlov V E Starik A M and Titova N S 2010 On the influence of singlet oxygen molecules on the speed of flame propagation in methane-air mixture *Combust. Flame* **157** 313–27

[14] Gudmundsson J T and Lieberman M A 2015 On the role of metastables in capacitively coupled oxygen discharges *Plasma Sources Sci. Technol.* **24** 035016

[15] Colonna G Esposito F Gorse C Hassouni K Laricchiuta A Longo S Capitelli M and Celiberto R 2016 *Fundamental Aspects of Plasma Chemical Physics: Kinetics* (Springer)

[16] Kustova E V and Puzyreva L A 2009 Transport coefficients in nonequilibrium gas-mixture flows with electronic excitation *Phys. Rev.* E **80** 046407

[17] Istomin V A, Kustova E V and Mekhonoshina M A 2014 Eucken correction in high-temperature gases with electronic excitation *J. Chem. Phys.* **140** 184311

[18] Istomin V A and Kustova E V 2017 State-specific transport properties of partially ionized flows of electronically excited atomic gases *Chem. Phys.* **485–486** 125–39

[19] Hirschfelder J O 1957 Heat conductivity in polyatomic or electronically excited gases. II *J. Chem. Phys.* **26** 282–5

[20] Tee L S, Gotoh S and Stewart W E 1966 Molecular parameters for normal fluids. Lennard-Jones 12-6 potential *Ind. Eng. Chem. Fundam.* **5** 356–63

[21] Hulburt H M and Hirschfelder J O 1941 Potential energy functions for diatomic molecules *J. Chem. Phys.* **9** 61–69

[22] Lim T C 2011 Application of extended-Rydberg parameters in general Morse potential functions *J. Math. Chem.* **49** 1086–91

[23] Richard B B 1979 *Atom—Molecule Collision Theory* (Springer)

[24] Child M 1985 Molecular potential energy functions *Phys. Bull.* **36** 507–507

[25] Tang K T and Toennies J P 1984 An improved simple model for the van der Waals potential based on universal damping functions for the dispersion coefficients *J. Chem. Phys.* **80** 3726–41

[26] Laporta V, Celiberto R and Wadehra J M 2012 Theoretical vibrational-excitation cross sections and rate coefficients for electron-impact resonant collisions involving rovibrationally excited N^2 and NO molecules *Plasma Sources Sci. Technol.* **21** 055–018

[27] Laporta V, Heritier K L and Panesi M 2016 Electron-vibration relaxation in oxygen plasmas *Chem. Phys.* **472** 44–49

[28] Buchowiecki M and Szabó P 2022 N-H collision integrals with study of repulsive interactions *Plasma Sources Sci. Technol.* **31** 045010

[29] Liu H, Shi D, Sun J, Zhu Z and Shulin Z 2014 Accurate calculations on the 22 electronic states and 54 spin-orbit states of the O_2 molecule: potential energy curves, spectroscopic parameters and spin-orbit coupling *Spectrochim. Acta* A **124** 216–29

[30] Robert J B, Sigrid D P and Miljenko P 1976 *Ab initio* vibrational analysis of the Schumann-Runge bands and the neighboring absorption region of molecular oxygen *Chem. Phys. Lett.* **42** 383–9

[31] Müller T, Dallos M, Lischka H, Dubrovay Z and Szalay P G 2001 A systematic theoretical investigation of the valence excited states of the diatomic molecules B_2, C_2, N_2 and O_2 *Theor. Chem. Acc.* **105** 227–43

[32] Hochlaf M, Ndome H, Hammoutène D and Vervloet M 2010 Valence–Rydberg electronic states of N_2: spectroscopy and spin–orbit couplings *J. Phys. B: At. Mol. Opt. Phys.* **43** 245101

[33] Qin Z, Zhao J and Liu L H 2019 Radiative transition probabilities between low-lying electronic states of N_2 *Mol. Phys.* **117** 1–16

[34] Ding Z, Qin Z and Liu L H 2023 Collision integrals for $N(^4S)$-$N(^4S)$, $N(^4S)$-$N(^2D)$ and $N(^4S)$-$N(^2P)$ interactions *Phys. Fluids* **35** 027127

[35] Nyeland C and Mason E A 1967 Adiabatic excitation transfer in gases: effects on transport *Phys. Fluids* **10** 985–91

[36] Sourd B, André P, Aubreton J and Elchinger M F 2007 Influence of the excited states of atomic nitrogen $N(^2D)$ and $N(^2P)$ on the transport properties of nitrogen. Part I: atomic nitrogen properties *Plasma Chem. Plasma Process.* **27** 35–50

[37] Laricchiuta A, Bruno D, Capitelli M, Celiberto R, Gorse C and Pintus G 2008 Collision integrals of oxygen atoms and ions in electronically excited states *Chem. Phys.* **344** 13–20

[38] Laricchiuta A, Capitelli M, Bruno D, Pirani F, Colonna G, Gorse C, Celiberto R, Catalfamo C and Terlizzi G 2008 The role of electronically excited states on transport properties of air plasmas *40th AIAA Thermophysics Conf.*

[39] Laricchiuta A, Pirani F, Colonna G, Bruno D, Gorse C, Celiberto R and Capitelli M 2009 Collision integrals for interactions involving atoms in electronically excited states *J. Phys. Chem.* A **113** 15250–6

[40] Biolsi L and Holland P M 2004 High temperature transport properties of dilute nitrogen atoms *Int. J. Thermophys.* **25** 1063–73

[41] Capitelli M and Ficocelli E 1972 Collision integrals of oxygen-atoms in different electronic states *J. Phys. B: At. Mol. Phys.* **5** 2066–73

[42] Friedrich H 2016 *Classical Scattering Theory* (Springer) pp 1–21

[43] O'hara H and Smith F J 1971 Transport collision integrals for a dilute gas *Comput. Phys. Commun.* **2** 47–54

[44] O'Hara H and Smith F J 1970 The efficient calculation of the transport properties of a dilute gas to a prescribed accuracy *J. Comput. Phys.* **5** 328–44

[45] Dalgarno A and McDowell M R C 1956 Charge transfer and the mobility of H^- ions in atomic hydrogen *Proc. Phys. Soc.* A **69** 615

[46] Herzberg G 1940 Molecular spectra and molecule structure. I. Diatomic molecules *J. Phys. Chem.* **44** 954–954

[47] Kevin P M 2022 *Probabilistic Machine Learning: An Introduction* (MIT Press)

[48] Werner H J *et al* 2020 The Molpro quantum chemistry package *J. Chem. Phys.* **152** 144107

[49] Werner H J, Knowles P J, Knizia G, Manby F R and Schütz M 2012 Molpro: a general-purpose quantum chemistry program package *Wiley Interdiscip. Rev.-Comput. Mol. Sci.* **2** 242–53

[50] Knowles P J and Werner H J 1985 An efficient second-order MCSCF method for long configuration expansions *Chem. Phys. Lett.* **115** 259–67

[51] Werner H J and Knowles P J 1988 An efficient internally contracted multiconfiguration–reference configuration interaction method *J. Chem. Phys.* **89** 5803–14

[52] Knowles P J and Werner H J 1988 An efficient method for the evaluation of coupling coefficients in configuration interaction calculations *Chem. Phys. Lett.* **145** 514–22

[53] Langhoff S R and Davidson E R 1974 Configuration interaction calculations on the nitrogen molecule *Int. J. Quantum Chem.* **8** 61–72

[54] Truhlar D G 1998 Basis-set extrapolation *Chem. Phys. Lett.* **294** 45–48

[55] Fast P L, Sanchez M L and Truhlar D G 1999 Infinite basis limits in electronic structure theory *J. Chem. Phys.* **111** 2921–6

[56] Kendall R A, Dunning T H and Harrison R J 1992 Electron affinities of the first-row atoms revisited. systematic basis sets and wave functions *J. Chem. Phys.* **96** 6796–806

[57] Woon D E and Dunning T H 1993 Gaussian basis sets for use in correlated molecular calculations. III. The atoms aluminum through argon *J. Chem. Phys.* **98** 1358–71

[58] Guberman S L 2012 Spectroscopy above the ionization threshold: dissociative recombination of the ground vibrational level of N_2^+ *J. Chem. Phys.* **137** 074309

[59] Ndome H, Hochlaf M, Lewis B R, Heays A N, Gibson S T and Lefebvre-Brion H 2008 Sign reversal of the spin-orbit constant for the $C^3\Pi_u$ state of N_2 *J. Chem. Phys.* **129** 164307

[60] Little D A and Tennyson J 2013 An ab initio study of singlet and triplet Rydberg states of N_2 *J. Phys. B: At. Mol. Opt. Phys.* **46** 145102

[61] Schaefer H F and Harris F E 1968 *Ab initio*calculations on 62 low-lying states of the O_2 molecule *J. Chem. Phys.* **48** 4946–55

[62] Brady R P, Yurchenko S N, Kim G S, Somogyi W and Tennyson J 2022 An *ab initio* study of the rovibronic spectrum of sulphur monoxide (SO): diabatic vs. adiabatic representation *Phys. Chem. Chem. Phys.* **24** 24076–88

[63] Zener C 1932 Non-adiabatic crossing of energy levels *Proc. R. Soc.* A **137** 696–702

[64] Baer M 2006 *Beyond Born-Oppenheimer: Electronic Nonadiabatic Coupling Terms and Conical Intersections* (Wiley)

[65] An H and Baeck K K 2015 A practical and efficient diabatization that combines Lorentz and Laplace functions to approximate nonadiabatic coupling terms *J. Chem. Phys.* **143** 194102

[66] Van T V, Kowalczyk T, Kaduk B, Wang L P, Cheng C L and Wu Q 2010 The diabatic picture of electron transfer, reaction barriers and molecular dynamics *Annu. Rev. Phys. Chem.* **61** 149–70

[67] Simah D, Hartke B and Werner H J 1999 Photodissociation dynamics of H_2S on new coupled ab initio potential energy surfaces *J. Chem. Phys.* **111** 4523–34

[68] Lofthus A and Krupenie P H 1977 The spectrum of molecular nitrogen *J. Phys. Chem. Ref. Data* **6** 113–307

[69] Oddershede J, Grūner N E and Diercksen G H 1985 Comparison between equation of motion and polarization propagator calculations *Chem. Phys.* **97** 303–10

[70] Su H, Cheng X, Cooper B, Tennyson J and Zhang H 2022 Electron-impact high-lying N_2^- resonant states *Phys. Rev.* A **105** 062824

[71] Moore C E 1970 Ionization potentials and ionization limits derived from the analyses of optical spectra *Technical Report* (National Standard Reference Data System)

[72] Krupenie P H 1972 The spectrum of molecular oxygen *J. Phys. Chem. Ref. Data* **1** 423–534

[73] Herzberg G and Huber K P 1979 *Molecular Spectra and Molecular Structure* (Springer)

[74] Saxon R P and Liu B 1977 A binitio configuration interaction study of the valence states of O_2 *J. Chem. Phys.* **67** 5432–41

[75] Moore C E 1993 *Tables of Spectra of Hydrogen, Carbon, Nitrogen, and Oxygen Atoms and lons* ed Gallagher J W (CRC Press)

[76] Ryabtsev A N, Kink I, Awaya Y, Ekberg J O, Mannervik S, Ölme A and Martinson I 2005 Additions to the spectrum and energy levels and a critical compilation of singly-ionized boron, B II *Phys. Scr.* **71** 489

[77] Zhu C and Nakamura H 1994 Theory of nonadiabatic transition for general two-state curve crossing problems. I. Nonadiabatic tunneling case *J. Chem. Phys.* **101** 10630–47

[78] Zhu C and Nakamura H 1995 Theory of nonadiabatic transition for general two-state curve crossing problems. II. Landau–zener case *J. Chem. Phys.* **102** 7448–61

[79] Hong Q, Bartolomei M, Pirani F, Esposito F, Sun Q and Coletti C 2022 Vibrational deactivation in $O(^3P)+N_2$ collisions: from an old problem towards its solution *Plasma Sources Sci. Technol.* **31** 084008

[80] Gudmundsson J T and Proto A 2019 Electron heating mode transitions in a low pressure capacitively coupled oxygen discharge *Plasma Sources Sci. Technol.* **28** 045012

[81] Swaminathan-Gopalan K and Stephani K A 2016 Recommended direct simulation Monte Carlo collision model parameters for modeling ionized air transport processes *Phys. Fluids* **28** 027101

[82] Boyd I D and Schwartzentruber T E 2017 *Nonequilibrium Gas Dynamics and Molecular Simulation* (*Cambridge Aerospace Series*) (Cambridge University Press)